Journal of Materials Chemistry A

ROYAL SOCIETY OF CHEMISTRY

REVIEW

View Article Online
View Journal | View Issue

Cite this: J. Mater. Chem. A, 2025, 13, 8939

A paradigm shift from traditional non-contact sensors to tele-perception

Jiaxin Guo,†[ab] Yan Du, †[ab] Zhonglin Wang[ac] and Di Wei *[ad]

With the rapid advancement of embodied perception technologies, the demand for enhanced interaction versatility, extended perceptual reach, and heightened sensitivity in human-machine interfaces (HMI) continues to grow. Triboelectric nanogenerator (TENG) based non-contact sensors have emerged as a transformative solution, offering exceptional adaptability while mitigating challenges such as mechanical degradation and potential health risks. However, achieving superior sensitivity and extending sensing ranges remain critical bottlenecks. Addressing these limitations, researchers have pioneered the concept of tele-perception, a groundbreaking innovation that breaks the limitations of traditional non-contact sensors by enabling precise, long-range perceptual capabilities. This review explores the paradigm shift from traditional non-contact sensors to tele-perception, highlighting the foundational principles, representative system architectures, and cutting-edge optimization strategies that define this new approach to sensing without physical interaction. Particular emphasis is placed on the integration of advanced charge-trapping mechanisms to enhance electrostatic charge stability and the deployment of intelligent algorithms and deep learning (DL) techniques to advance tele-perception functionalities. Concluding with an analysis of the challenges and future opportunities in tele-perception systems development, this review offers critical insights to guide next-generation research and applications in this transformative field.

Received 28th December 2024
Accepted 24th February 2025

DOI: 10.1039/d4ta09222h

rsc.li/materials-a

1 Introduction

With the rapid advancements in embodied intelligence, the interaction between humans and their environment is undergoing a profound transformation. Embodied perception emphasizes dynamic, integrated interactions between perception and action, driving global progress in efficiency and cognitive capabilities.[1–3] Intelligent systems, such as computers, robotics, and sensors, are central to this transformation, redefining the landscape of HMI.[4–7] Among these advancements, tactile perception is pivotal in enabling robots to autonomously perceive, decide, and adapt to complex environments, becoming a core driver of cognitive systems and robotics.[8,9] However, conventional tactile contact sensing is limited by challenges such as wear and potential health risks.[10,11] Consequently, non-contact sensing technology has emerged as a promising alternative, offering a sustainable and efficient solution for tactile perception, thereby expanding the avenues and capabilities of HMI.

Traditional non-contact sensing technologies, including visual,[12–15] ultrasonic,[16–19] light detection and ranging (LiDAR),[20–22] infrared,[23–27] electromagnetic,[28,29] and capacitive sensors,[30–34] have advanced significantly to meet modern demands. Visual sensors deliver detailed image and video data but are limited by lighting conditions. Ultrasonic and LiDAR sensors excel in long-distance detection, with LiDAR offering wide-range scanning and high precision, though at a high cost. Infrared sensors provide fast thermal detection but are sensitive to temperature fluctuations. Electromagnetic sensors, such as magnetic and capacitive types, offer high precision and adaptability in complex environments. Magnetic sensors detect magnetic field changes *via* the Hall effect, while capacitive sensors deliver high-precision, short-range proximity detection with adjustable sensitivity. However, significant challenges remain. Reliance on external power sources restricts energy efficiency and operational lifespan. Sensitivity and accuracy are influenced by material properties, design limitations, and environmental variables, which compromise performance under complex conditions. Furthermore, limited integration capabilities, lack of multifunctionality, and high production costs impede scalability and broader adoption.[35–39] TENGs provide a promising solution by converting ambient

[a]Beijing Institute of Nanoenergy and Nanosystems, Chinese Academy of Sciences, Beijing 101400, China
[b]School of Nanoscience and Engineering, University of Chinese Academy of Sciences, Beijing 100049, China
[c]Beijing Key Laboratory of Micro-Nano Energy and Sensor, Center for High-Entropy Energy and Systems, Beijing Institute of Nanoenergy and Nanosystems, Chinese Academy of Sciences, Beijing 101400, P. R. China
[d]Centre for Photonic Devices and Sensors, University of Cambridge, 9 JJ Thomson Avenue, Cambridge, CB3 0FA, UK. E-mail: dw344@cam.ac.uk
† These authors contributed equally to this work.

mechanical energy into electrical signals, eliminating the need for external power. In addition, TENG exhibits simplicity, cost-effectiveness, diverse application scenarios and high conversion efficiency under low-frequency conditions, making them suitable for non-contact sensing applications.[40–45] When integrated with sensors, TENGs enable self-powered, portable systems for applications like gesture recognition,[46–48] non-contact interfaces,[49,50] joint motion[51] and gait monitoring.[52–54] These systems perform reliably in dynamic environments, offering scalable, sustainable solutions for next-generation intelligent sensing technologies.

Traditional non-contact sensors based on TENG, despite their advantages, face significant challenges in output performance, primarily due to the limited charge generated by electrostatic induction. A key difficulty lies in charge-trapping, as the retention of triboelectric charges becomes increasingly difficult. As the separation distance grows, the inability to effectively trap charges leads to a further decline in output performance, thereby restricting the sensing range.[55–58] To address these challenges, research has primarily focused on material composite design, chemical modification and structural optimization. For instance, Park *et al.*[59] improved output performance by incorporating laser-carbonized MXene/ZiF-67 nanocomposites as a charge trapping layer, while Xu *et al.*[60] achieved long-distance sensing using MXene/silicone composites. However, these advancements still face limitations in sensing range and require larger devices for long-distance detection.[61] Additionally, challenges persist in sensitivity adjustment and threshold setting, which are critical for accurate detection across varying distances. Recent work by Wei *et al.*[62] demonstrated human presence detection at distances of up to 155 cm by structured doping of inorganic nanoparticles to create charge traps. This design achieved a sensitivity of $\Delta V/\Delta d = 142\ \mathrm{V\ cm^{-1}}$, significantly surpassing current technological standards. The key innovation involved doping inorganic non-metallic nanoparticles (SiO_2, TiO_2, $BaTiO_3$ and $SrTiO_3$) into the structure of TENGs to improve electrostatic charge-trapping ability and stabilize charge retention, thereby addressing the challenge of maintaining charge stability in traditional non-contact TENGs. In addition, the integration of adaptive pulse identification technology and long short-term memory (LSTM) networks significantly enhanced the robustness, adaptability, and accuracy of the tele-perception system. Two-dimensional sensor matrix was employed to integrate real object scanning data into a convolutional neural network (CNN), enabling the multi-receptor skin to effectively function in real-world

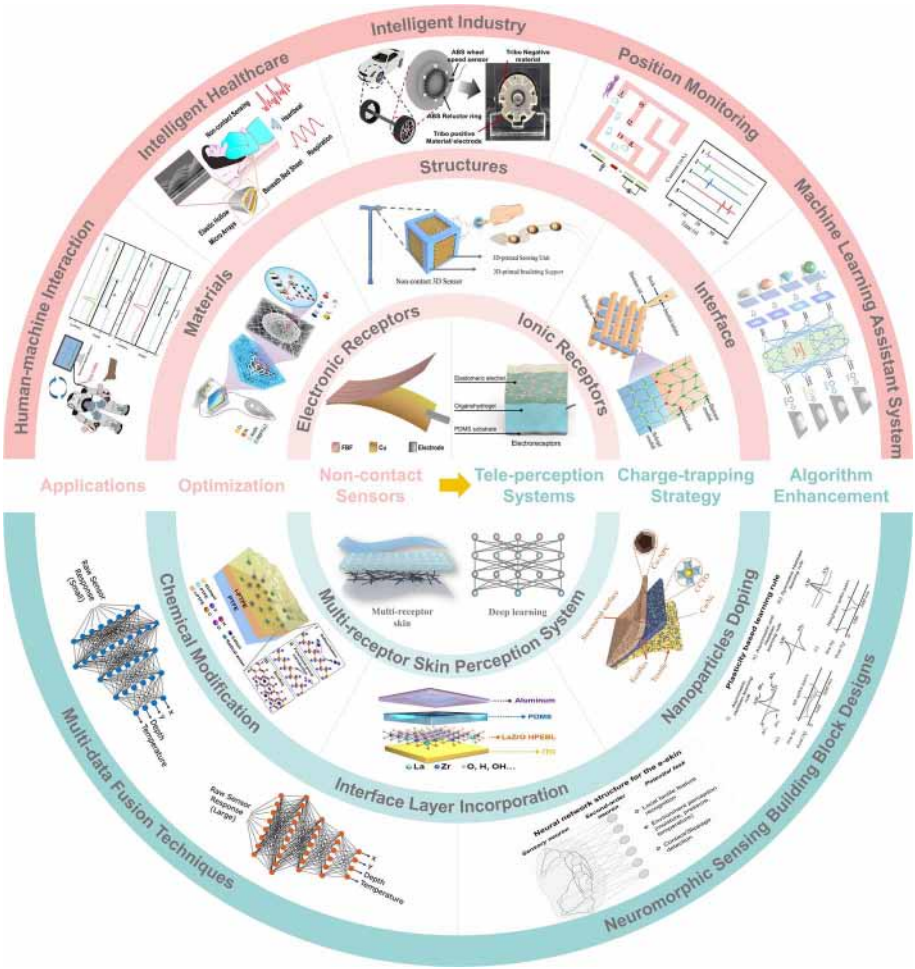

Fig. 1 An overview of the latest advancements of traditional non-contact sensors and tele-perception systems.

applications, thereby improving target recognition and overall system performance. This breakthrough highlights the necessity of extending sensing capabilities beyond physical contact, laying a strong foundation for the continued evolution of tele-perception. Fully realizing the potential of tele-perception necessitates a fundamental paradigm shift, from traditional non-contact sensors to adaptive embodied intelligent systems. Tele-perception itself embodies this transformation, redefining the landscape of interaction by enabling long-range, high-precision sensing and facilitating more dynamic context awareness HMI.

This review explores the paradigm shift[63] from traditional non-contact sensors to tele-perception. We begin by presenting two primary types of traditional non-contact sensors based on TENG: electronic receptors and ionic receptors, with a focus on their operating principles, typical architectures, performance optimization strategies, and applications. The concept of tele-perception is then introduced, emphasizing the critical role of charge-trapping strategies in enhancing charge capture, transport efficiency, and long-term stability, alongside a particular focus on algorithm integration and optimization. Subsequently, recent advancements in traditional non-contact sensors and tele-perception systems are examined, highlighting their applications in HMI, intelligent monitoring, and machine learning assistant systems, as shown in Fig. 1. Moreover, various properties of non-contact sensors, including the latest advancements in tele-perception technologies, are compared in Table 1. This comparison highlights the improvements in sensitivity, charge retention, and sensing range, and underscores the integration of cutting-edge techniques. The review concludes by addressing the current technical challenges and outlining potential future research directions for tele-perception, particularly in the areas of advanced electrostatic charge-trapping strategies, collaborative algorithm optimization, and multifunctional integrated designs. By synthesizing these developments, we aim to provide a comprehensive resource for advancing tele-perception and promoting its broader integration into embodied intelligence systems.

2 Traditional non-contact sensors based on TENG

2.1 Principle of operation

Non-contact sensors based on TENG, as innovative sensing devices, can convert mechanical energy into electrical signals without the need for an external power source, operating in a completely contactless manner. This review focuses on two prevalent mechanisms: electronic receptors and ionic receptors, each characterized by unique features that make them suitable for specific application scenarios. Despite these differences, both mechanisms rely on the fundamental principle of electrostatic induction. When the relative position of the triboelectric layer shifts, the charge distribution is altered due to electrostatic induction. For instance, in everyday life, negative charges tend to accumulate on the surface of the human body due to the triboelectric interaction between the ground and shoes, with additional charges often concentrating at the fingertips due to the tip effect.[79,80] When a finger approaches the device in a non-contact manner, the redistribution of surface charges occurs through electrostatic induction. This process generates electric output signals in the external circuit. The operating principles of electronic and ionic receptors are compared in detail, as illustrated in Fig. 2, providing a theoretical foundation for understanding their respective applications.

Table 1 Summary and comparison of non-contact sensors reported in literatures

	Dielectric material	Electrode material	Approaching object	Sensing range (cm)	Sensitivity (V cm^{-1})	Reference
1	Ionic hydrogel	Ionic hydrogel/PDMS	Finger	4	—	64
2	Printing paper	Copper	People	100	0.15	61
3	CNF–Mxene	Cu	Finger	50	0.9	65
4	FEP	ITO/PET	Human hand	250	1	66
5	F-TiO_2	Cu	Robot arm	300	1.4	67
6	PTFE	Cu	Human hand	11	3.15	68
7	MXene/silicone, LC-MXene/ZiF-67 nanocomposites	Ag coated conductive fabric	Human hand	2	3.5	59
8	Siloxene/Ecoflex	Cu	Nitrile glove	14	4.38	69
9	PDMS/SiO_2	Organohydrogel	PTFE	9	4.7	70
10	PVDF/$Ti_3C_2T_x$	Cu	Nylon film	70	5	71
11	MXene/silicone	Conductive sponge	Nylon film	200	5	60
12	PDMS–PTFE and TPU–SiO_2 composite film	Al	PDMS–PTFE and TPU–SiO_2	0.3	5.1	72
13	Co–NPC/Ecoflex	Silver-coated conducting fabric	Human hand	20	5.6	73
14	PI-*b*-C_{60}	Ag/PDMS/Au and Al	Finger	0.4	8.2	74
15	Fish bladder film (FBF)	Cu	FEP	2.7	34.9	75
16	PET	EIPG	Human hand	10	43	76
17	PTFE	Ag/polyamide	Polyamide	18	56	77
18	Bi_2Se_3/S.R. and carbonized textile	Ag NWs	Nylon	1	58	78
19	PDMS/PTFE/$SrTiO_3$	Ag NWs	Nylon/PTFE/FEP	155	142	62

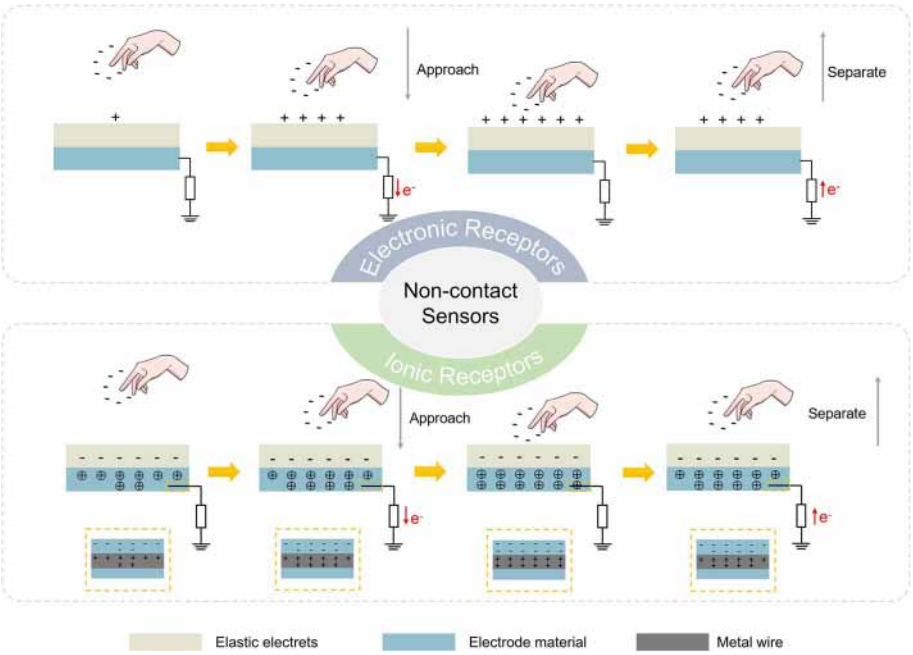

Fig. 2 The operating principles of traditional non-contact sensors including electronic receptors and ionic receptors.

The detailed working mechanism of the sensors can be outlined in the following stages. In electronic receptors, the finger initially maintains a specific distance from the device surface, inducing a small amount of positive charge on the device due to electrostatic induction. As the finger approaches the device, additional positive charges accumulate to neutralize the negative charge on the finger. This results in a potential difference that drives free electrons from the electrode to the ground through an external circuit, generating an output current signal. As the finger draws closer, the induced positive charges on the device surface fully screen the negative charges, achieving electrostatic equilibrium. Conversely, as the finger moves away, the process reverses, causing the charge flow to change direction and completing a full signal cycle. In contrast to traditional electronic devices based on electronic conduction, ionic receptors primarily function through ion movement, making them more akin to the electrical signaling mechanisms found in biological systems.[81–83] In this case, the electret layer in ionic receptors is initially pre-charged with negative charges. As a result, cations accumulate in the ionic electrode layer beneath the electret, neutralizing the electric field generated by the electret and achieving electrostatic equilibrium. Simultaneously, an electrical double layer (EDL)[84] forms at the interface between the metal wire and the ion electrode due to the polarization effect, inducing an equal amount of anions. As the finger approaches the device, the cation concentration on the ion electrode surface increases, creating an electric field that neutralizes the negative charge on the finger, achieving balance. Concurrently, the anion concentration in the EDL rises, driving electron flow from the metal wire to the ground through an external circuit. As the finger draws closer, the cation concentration continues to rise until the finger's negative charge is fully neutralized, reaching electrostatic equilibrium. Conversely, as the finger moves away, the cation concentration gradually decreases, disrupting the charge balance and generating a reverse current signal. Through this cyclic process, periodic electrical signal fluctuations are induced as the finger moves closer or farther, enabling highly sensitive mechanical signal detection.

2.2 Electronic receptors

2.2.1 Typical structures. The structural design significantly impacts the device performance. For the traditional non-contact sensors based on TENG, factors including the relative position of the electrode and triboelectric layer, material selection, geometric dimensions and support structure directly influence reliability, robustness, response range and sensitivity.[85–87] An optimized structure not only enhances performance but also improves installation efficiency and adaptability, facilitating seamless integration into complex environments and ensuring conformity to irregular surfaces.[88] Optimizing the contact area and electric field distribution between the triboelectric layer and electrode improves output power and signal strength, enabling high-precision detection and better performance in various applications. Currently, in addition to the most common planar and stacked structures, several other notable configurations, such as spring and origami structures, have been developed for electronic receptors.

The most common planar structure consists of a triboelectric charge generation layer and an electrode layer. This simple design enables devices to respond sensitively to external mechanical energy. Reducing the number of layers makes the devices lighter, thinner and more flexible, significantly improving its bendability. These features make it ideal for

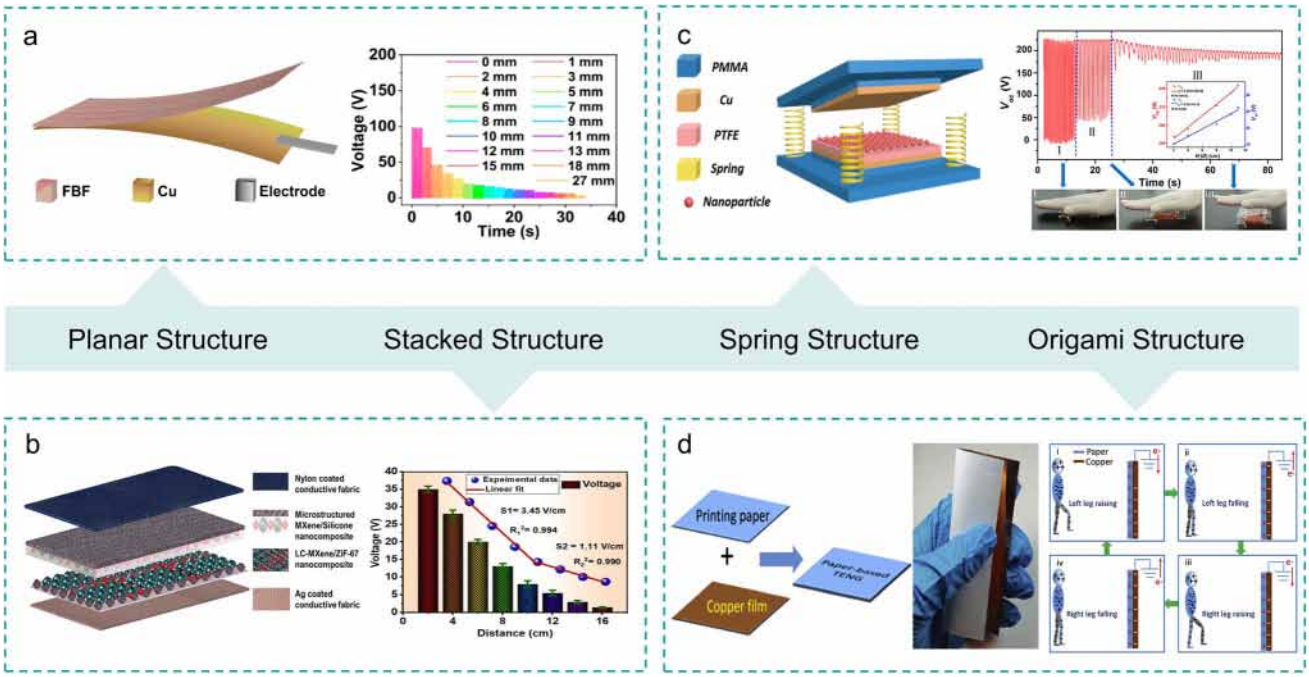

Fig. 3 Typical structures of electronic receptors. (a) Representative planar structure diagram of electronic receptors and the response curve with different starting points (0–2.7 cm). Reproduced from ref. 75 with permission from American Chemical Society, copyright 2020. (b) Representative stacked structure diagram of electronic receptors embedded with the laser-carbonized Mxene/ZiF-67 nanocomposite and the electrical output performance with a varying distance. Reproduced from ref. 59 with permission from Elsevier, copyright 2022. (c) Representative spring structure diagram of electronic receptors and application in position monitoring. Reproduced from ref. 68 with permission from American Chemical Society, copyright 2018. (d) Representative origami structure diagram of electronic receptors and principle of human motion monitoring. Reproduced from ref. 61 with permission from Elsevier, copyright 2020.

applications requiring high flexibility, such as wearable devices and electronic-skin (e-skin). For example, Cao *et al.*[75] developed a fish bladder film-based TENG that integrated the advantages such as multifunctionality, ultra-flexibility and high sensitivity. In addition, the device demonstrated non-contact sensing capabilities within a range of 0–2.7 cm, making it ideal for applications such as HMI, smart systems, and prosthetics control (Fig. 3a). The planar structure forms the foundation for other device designs based on TENG, serving as a basis for the development and optimization of diverse structures and applications. In contrast, the stacked structure includes an additional intermediate layer, which typically serves as a charge-generating surface to enhance charge collection, while also functioning as both a charge transfer and storage layer. The charge transfer layer mitigates charge accumulation on the triboelectric surface and captures electrons within the space charge region, thereby extending the detection range. For example, Park *et al.*[59] employed laser-carbonized MXene/ZiF-67 nanocomposite as an intermediate layer, achieving a charge density of 15.3 μC m^{-2} and stable output performance up to 2 cm (Fig. 3b). This approach represents an innovative and effective strategy for designing high-performance devices in self-powered systems and sensing applications. Sensors with spring structures, in particular, demonstrate heightened sensitivity to subtle environmental disturbances or object displacements, owing to their exceptional flexibility and recoverability. In non-contact mode, even minor displacements or mechanical stimuli can be detected in real-time through variations in electrical signals, showcasing excellent sensitivity and rapid response times. For example, Cao *et al.*[68] developed a non-contact, self-powered positioning and motion tracking system based on the spring structure, capable of detecting small movements at heights of 1–11 cm, with a sensitivity of approximately 3.15 V cm^{-1} (Fig. 3c). The origami structure, an innovative variation of the planar design, incorporates the human body as a functional component, with other parts made of printed paper and metal electrodes. This design integrates the advantages of light weight, low cost, and ease of fabrication, providing an optimal solution for lightweight and cost-effective TENG applications. For example, Shi *et al.*[61] proposed the non-contact paper-based TENG, demonstrating that the output voltage signal directly reflected the walking gait cycle (leg raising and falling), movement direction, walking or running speed and movement path (Fig. 3d). Overall, these structural innovations have advanced TENG technology and paved the way for more efficient and intelligent sensor systems.

Each structure offers distinct advantages: the planar structure is simple, lightweight, and well-suited for wearable applications; the stacked structure enhances the detection range; the spring structure delivers high sensitivity and rapid response, making it ideal for positioning and motion tracking; and the origami structure incorporates the human body as part of the device, offering low cost and the ability to directly capture motion data. These innovative structural designs provide strong

support for the diverse applications of non-contact sensors based on TENG across a wide range of scenarios.

2.2.2 Performance optimization. While an optimized structure can improve the electrical output, mechanical stability, and durability of traditional non-contact sensors based on TENG, their electrical performance remains inferior to that of contact-mode sensors. Moreover, the output decreases further as the separation distance increases. This is primarily due to the limited number of charges generated by electrostatic induction, with surface charges on the rough triboelectric layer gradually decaying.[89] The reduced electrical output during non-contact operation constrains the wider application of these devices in energy harvesting and proximity sensing. To address this limitation, researchers have proposed various strategies to optimize electrical performance. This section reviews and discusses approaches such as material composite design, chemical modification, and structural optimization, aiming to provide valuable insights for enhancing the electrical output and expanding the application potential of non-contact sensors.

Material composite design focuses on enhancing charge capture capabilities by selecting appropriate triboelectric materials to increase charge density and precisely tuning the interfacial electrical and chemical properties through doping. This approach significantly enhances device performance by optimizing charge generation and collection efficiency.[90] Among various triboelectric materials, MXene is notable for its high electronegativity, decent conductivity and superior charge capture capability, leading to widespread applications.[91–96] A novel laser-carbonized MXene/ZiF-67 nanocomposite fabricated *via* a simple laser processing technique was developed by Park *et al.*,[59] which integrated the unique porous structure of ZiF-67, enabling high output performance and stable operation in both contact and non-contact modes (Fig. 4a). Nie *et al.*[67] proposed a hierarchical spatial assembly strategy for a double-layer functionalized triboelectric material, which significantly improves humidity stability. Electrophoretic deposition was used to achieve the layered spatial assembly, incorporating MXene filler as an intermediate charge storage layer, enhancing

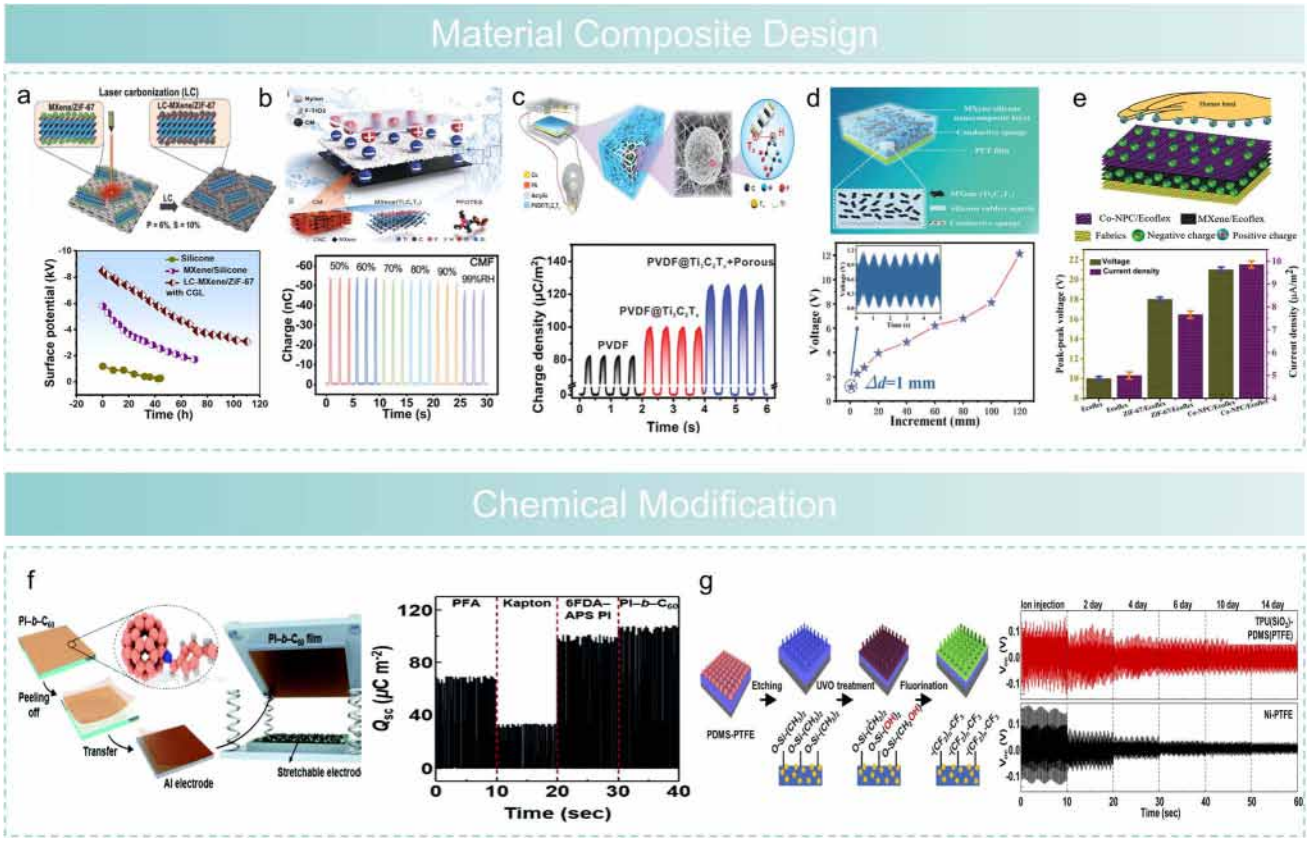

Fig. 4 Performance optimization of electronic receptors. Material composite design: (a) laser carbonized Mxene/ZiF-67 nanocomposites as an intermediate layer to improve the output performance of fabric-based TENG. Reproduced from ref. 59 with permission from Elsevier, copyright 2022. (b) Schematic diagram of CMF-TENG-based sensor in a humid environment with MXene filler as an intermediate charge storage layer. Reproduced from ref. 67 with permission from Wiley-VCH, copyright 2024. (c) Non-contact sensor based on a polyvinylidene fluoride@Mxene ($Ti_3C_2T_x$) composite film with sphere multi-physical network structure. Reproduced from ref. 71 with permission from Wiley-VCH, copyright 2022. (d) Ultra-long distance detection and high sensitivity self-powered non-contact sensor based on MXene composites. Reproduced from ref. 60 with permission from Wiley-VCH, copyright 2023. (e) Cobalt nanoporous carbon functionalized nanocomposites for non-contact sensing. Reproduced from ref. 73 with permission from Wiley-VCH, copyright 2021. Chemical modification: (f) sustainable high-charge C_{60}-functionalized polyimide for non-contact sensing. Reproduced from ref. 74 with permission from Royal Society of Chemistry, copyright 2021. (g) The schematic diagram of a sustainable charging composite material with amphiphilic surface prepared by reactive ion etching and fluorination treatment. Reproduced from ref. 72 with permission from Elsevier, copyright 2023.

the signal intensity and accuracy of the triboelectric material (Fig. 4b). In addition, a polyvinylidene fluoride (PVDF)@$Ti_3C_2T_x$ triboelectric material with a spherical multi-physical network was developed to efficiently capture and accumulate negative charges.[71] The highly conductive $Ti_3C_2T_x$ was uniformly distributed within the microspheres, forming multiple interfaces and continuous conductive paths, significantly improving output performance and stability (Fig. 4c). Xu *et al.*[60] proposed a self-powered non-contact TENG (SNC-TENG) comprising MXene/silicone nanocomposites and a fully embedded conductive sponge. The complete embedding of the conductive sponge within the dielectric layer increased the effective electrode area in the electrostatic field, thereby enhancing the electrostatic induction effect. This design endowed the non-contact sensor with high sensitivity and an ultra-long detection range, enabling it to detect human activities at distances of up to 200 cm (Fig. 4d). The selection of triboelectric materials is fundamentally the most effective approach to enhance output performance.[97,98] However, it is constrained by the limited availability of high-performance materials. To further enhance performance, functional treatments such as doping can be applied to specific materials, optimizing their triboelectric properties. For example, a cobalt nanoporous carbon (Co–NPC)/Ecoflex with MXene/Ecoflex nanocomposite layer was developed for meeting the ongoing demand of tribo-negative materials, where Co nanoparticles uniformly distributed throughout the NPC matrix's spatial network.[73] The porous structure of the Co–NPC offered a high surface area for the nanocomposite, while the charge storage layer of the MXene/Ecoflex nanocomposite accumulated more negative charge, significantly enhancing the device output performance (Fig. 4e). Additionally, chemical modification through functional groups grafting and fluorination processes offers effective approaches to enhance triboelectric charge density, aiming to regulate charge distribution on material surfaces, manipulate charged groups or binding energy and enhance interface properties, achieving high output performance. Lee *et al.*[74] reported a non-contact device based on a novel dielectric of C_{60}-containing *block* polyimide (PI-*b*-C_{60}), achieving high output power and reliable operation due to the excellent charge retention properties and highly negative electrostatic potential of C_{60} (Fig. 4f). Baik *et al.*[72] functionalized PDMS–PTFE composites by etching and fluorination to create amphiphobic surfaces. The etching process introduced micro/nano hierarchical structures to create rough surface with air bubbles, while the subsequent fluorination further incorporated low-surface-energy fluorine groups, endowing the material with excellent water and oil repellency. These surface characteristics effectively suppressed charge dissipation caused by surface conductivity under high humidity or contaminated environments, significantly enhancing the material's charge retention capability and environmental adaptability, thereby improving the device's stability under harsh conditions (Fig. 4g).

Surface structure optimization is a universal and direct strategy that focuses on creating surface microstructures to enhance the effective triboelectric contact area.[99–101] This approach facilitates charge accumulation and distribution, thereby improving electrical performance, output efficiency, and stability across a wide range of materials and applications. Etched PTFE nanoparticle arrays[68] were employed to significantly enhance the effective contact surface and triboelectric charge density of the non-contact sensors, achieving an output of 222 V and 18 μA with improved sensitivity for non-contact sensing (Fig. 5a). Zhang *et al.*[65] employed a freeze-drying assisted 3D printing technique to construct a deep-trap layered structure of cellulose nanofiber (CNF) and MXene. Incorporating MXene nanosheets created open pores in the printed scaffold and enhanced the electrical performance of non-contact sensor (Fig. 5b). Chen *et al.*[77] proposed a bionic-antennae-array (BAA) sensor inspired by cockroach antennae, representing another innovative structural design. By leveraging the amplification effect of the antenna array, the BAA sensor achieved a detection range of 18 cm, a displacement resolution of 0.1 cm, and a sensitivity of 56 V cm^{-1}, demonstrating excellent performance in detecting the movement of non-contact objects (Fig. 5c). Zhong *et al.*[66] designed a megascopic air-bubble structure to enhance charge storage stability and recovery capability in devices using the heterocharge-synergy effect in electrets. And the multilayer electret film strengthened the electric field *via* the electrostatic field superposition effect, enabling an ultra-wide sensing range of over 250 cm in harsh environments (Fig. 5d). Yang *et al.*[76] demonstrated a flexible, transparent sensor with layered micro–nano textures, which increased the output signal by over 200%, significantly enhancing the device sensitivity (Fig. 5e).

The three aforementioned strategies, material composite design, chemical modification and structural optimization, effectively enhance traditional non-contact sensors' performance. Each method has distinct advantages and inherent limitations. Selecting appropriate triboelectric materials to fundamentally enhance performance is among the most effective strategies for improving output performance. However, this strategy is typically limited to specific material systems. Not all materials satisfy the requirements for high electronegativity and charge capture capability, making it challenging to identify perfectly suitable materials for specific applications. While modification moderately expands the material selection range and enhances design flexibility, its complexity significantly increases preparation costs and technical challenges. For example, uneven fluorination during the process may result in inconsistent surface characteristics, adversely affecting output stability and consistency. Additionally, chemical modification may introduce side effects, such as adverse impacts on the material's mechanical or electrical properties, requiring careful evaluation and optimization. Creating a surface microstructure efficiently increases the contact area of the triboelectric layer and reduces the air gap, preventing charge deposition and accumulation on the surface. This common and direct method improves charge capture ability and charge density, and is not limited by material characteristics, making it broadly applicable. However, improper structural design may affect the device long-term stability and service life. In summary, these three methods have distinct advantages and can complement each other in suitable application scenarios. In practice,

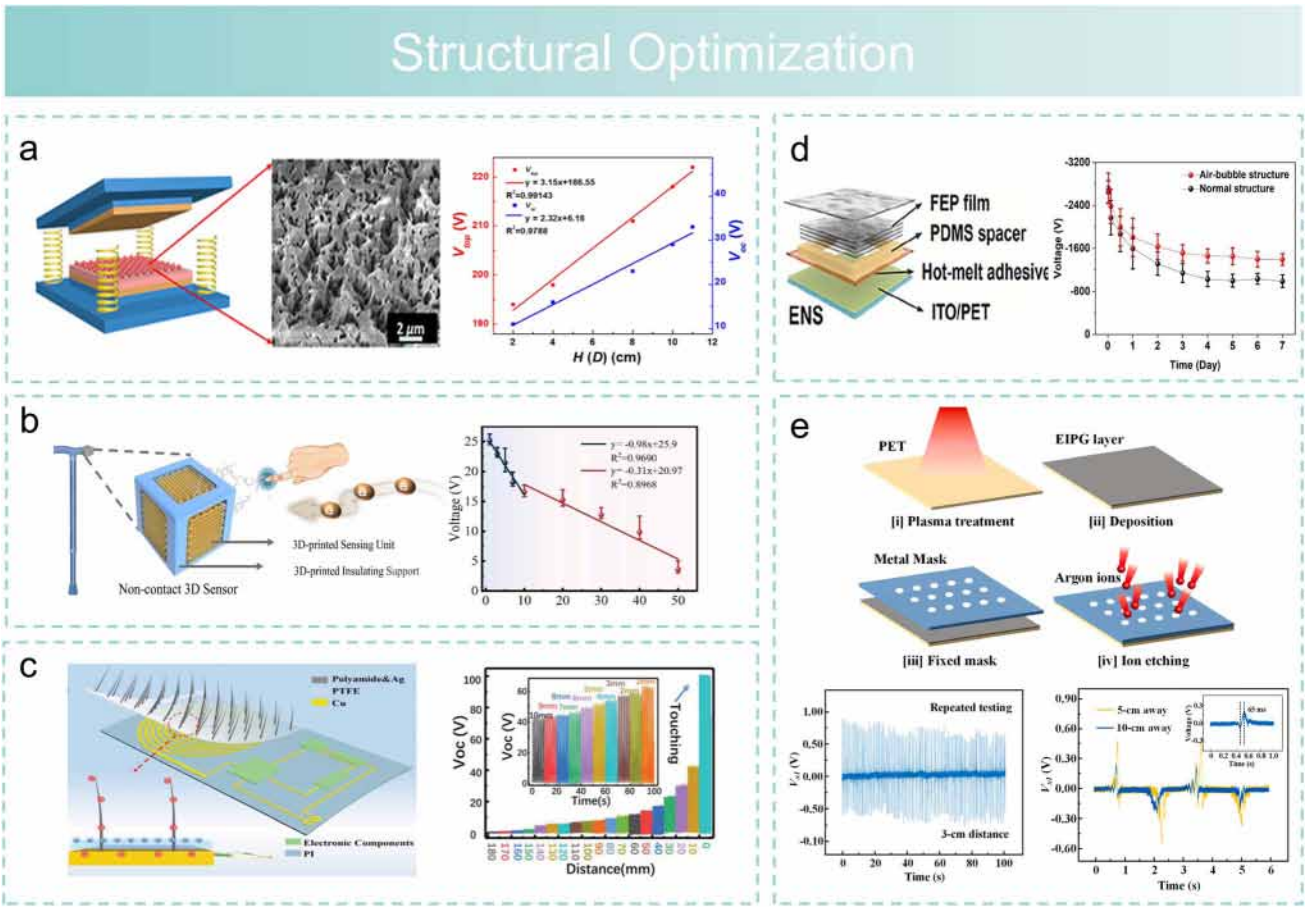

Fig. 5 Performance optimization of electronic receptors. Surface structure optimization: (a) the nano-particle array structure of PTFE formed by etching improves the sensitivity of the non-contact sensor to about 3.15 V cm^{-1}, and the sensing range is from 1 to 11 cm. Reproduced from ref. 68 with permission from American Chemical Society, copyright 2018. (b) A deep trap hierarchical structure based on CNF/MXene was fabricated by freeze-drying assisted 3D printing method, showing excellent sensing performance in multi-directional motion monitoring. Reproduced from ref. 65 with permission from Elsevier, copyright 2022. (c) The BAA sensor for non-contact motion recognition with a maximum sensing distance of 18 cm, a displacement resolution of 0.1 cm and a maximum sensitivity of approximately 56 V cm^{-1}. Reproduced from ref. 77 with permission from Wiley-VCH, copyright 2019. (d) The self-powered electret non-contact sensor with a large bubble structure achieves an ultra-wide sensing range of more than 250 cm. Reproduced from ref. 66 with permission from American Chemical Society, copyright 2023. (e) The flexible transparent sensor with layered micro–nano texture achieves higher sensitivity, and the output signal is increased by more than 200%. Reproduced from ref. 76 with permission from Elsevier, copyright 2021.

method selection should comprehensively consider the requirements and constraints of specific application scenarios to achieve optimal performance and meet diverse field needs.

2.3 Ionic receptors

2.3.1 Typic structures. Ionic receptors utilize dielectric materials such as hydrogels, ionic gels, and ionic liquids, which exhibit high sensitivity,[102,103] responsiveness,[104] flexibility,[105–108] and potential self-healing capabilities,[109–111] features that are difficult to achieve with electronic receptors. The structure of ionic sensors is relatively simple, typically classified into laminated and parallel configurations. The laminated structure consists of a basic triboelectric layer, an electrode layer, and a packaging layer. This multilayer design allows for the flexible integration of various functional materials, enhancing the sensor's performance and adaptability. Pu *et al.*[70] developed an artificial electroreceptor for proximal detection featuring this structure, comprising a pre-charged elastic electret, a conductive organic hydrogel as an ion electrode and an encapsulated silicon substrate layer. The elastic electret enabled the artificial electroreceptor to encode environmental pre-contact information into voltage pulses, generating significant electrical output *via* electrostatic induction when a naturally charged external target approached, acting as a unique pre-contact HMI (Fig. 6a). Zhou *et al.*[112] integrated ureido-based ionic liquid into hydrogel matrices to fabricate a multilayer composite electrode for non-contact electrocardiogram equipment (ECG), facilitating high-fidelity signal acquisition without significant noise artifacts and highlighting its importance in biosensors (Fig. 6b). The parallel structure, resembling a parallel plate capacitor, consists of two parallel electrode plates separated by a layer of ionic conductive material. The electrode plates can be fabricated from either flexible or rigid materials, while the ionic conductive materials encompass ionic gels, ionic liquids, and other similar substances. Mao *et al.*[64] reported a non-contact screen

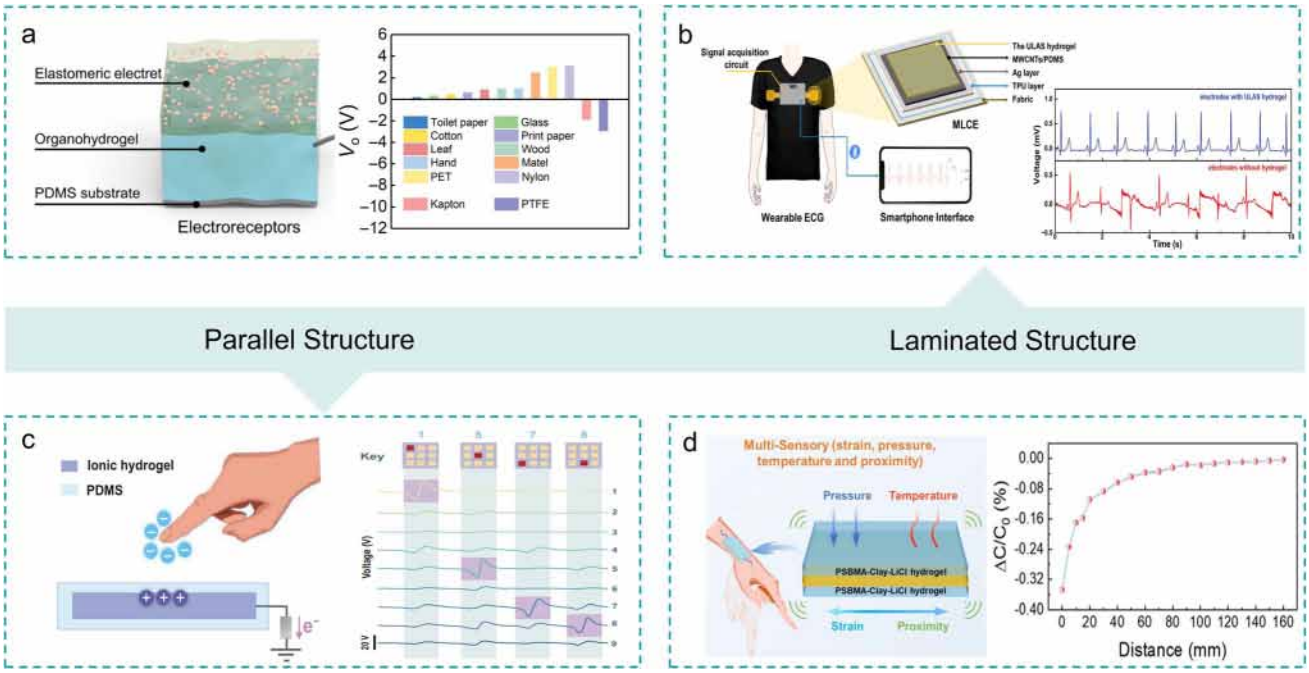

Fig. 6 Typical structures of ionic receptors. Representative laminated structure of ionic receptors: (a) the structure and the applicability for different materials of the artificial receptor. Reproduced from ref. 70 with permission from the American Association for the Advancement of Science, copyright 2022. (b) Diagram of the wearable ECG monitoring system and different signals detected in sleep heart detection. Reproduced from ref. 112 with permission from Wiley-VCH, copyright 2024. Representative parallel structure of ionic receptors: (c) schematic illustration of the working mechanism for the on-skin touchless screen sensor (OTSS) and application of screen operating system based on the OTSS units during the unlocking process. Reproduced from ref. 64 with permission from Tsinghua University Press, copyright 2023. (d) Schematic illustration of the fabricated PSBMA–clay–LiCl (PSCL) hydrogels and applications and performance that varies with finger proximity. Reproduced from ref. 113 with permission from Elsevier, copyright 2022.

sensor based on TENG, featuring an ionic hydrogel fully encapsulated in PDMS. This design provides stretchability while protecting the hydrogel from damage and dehydration (Fig. 6c). Chen *et al.*[113] developed a multifunctional hydrogel sensor with enhanced environmental adaptability and durability. By incorporating a dielectric layer between two hydrogel layers, the sensor achieved outstanding multi-sensory capabilities, enabling non-contact finger writing recognition (Fig. 6d).

2.3.2 Performance optimization. In sensors based on ionic receptors, gels play a critical role, offering properties such as softness, deformability, and biocompatibility. These attributes enable innovative applications that are not feasible with rigid electronic products, highlighting their significant potential in multifunctional iontronics.[114–116] However, retaining excessive solvated electrolytes within the polymer network remains a challenge, leading to environmental instability issues such as liquid leakage or evaporation.[117–119] Additionally, challenges such as stabilizing adhesion between hydrogel and elastomer layers,[120–122] ensuring low tackiness for smooth operation, preventing contamination, and achieving high output performance are yet to be fully resolved. Addressing these issues is crucial for enabling practical, everyday applications. This section explores strategies for optimizing ionic receptor performance, focusing on material selection, design considerations, and interface modifications, with the goal of improving stability, extending service life, and enhancing overall performance in real-world applications.

Material selection and design focus on constructing conductive nanochannels and achieving molecular synergies. When combined with dynamic cross-linked networks, these materials create synergistic effects that prevent liquid leakage or evaporation, thereby enhancing structural integrity and environmental adaptability. Wu *et al.*[123] introduced an intrinsically stretchable conductor in which small-molecule liquid electrolytes, such as ionic liquids, served as charge carriers. Polymers with ionic structures, such as polyzwitterions, enhanced ionic synergy with liquid electrolytes, forming conductive nanochannels and reducing electrolyte aggregation or leakage risks (Fig. 7a). Zhou *et al.*[112] employed molecular design to introduce hydrogen bonds and electrostatic interactions at the matrix–hydrogel interface, imparting excellent self-adhesive properties to the ionic hydrogel system (Fig. 7b). Additionally, dynamically crosslinked dry ICE was introduced for soft ionic electronics.[124] Without liquid molecules, ICE and related ionic electronic devices demonstrated excellent stability and functioned across a broad temperature range (Fig. 7c). Jia *et al.*[125] introduced another type of ICE, consisting of copolymer networks that hosted lithium cations and associated anions through lithium bonds and hydrogen bonds. Consequently, these materials exhibited inherent resistance to leakage and evaporation (Fig. 7d). Enhancing adhesion depends on interface modification, a direct approach emphasizing chemical anchoring *via* covalent crosslinking interactions to establish reliable interfacial bonding. Sun *et al.*[126] established covalent and robust

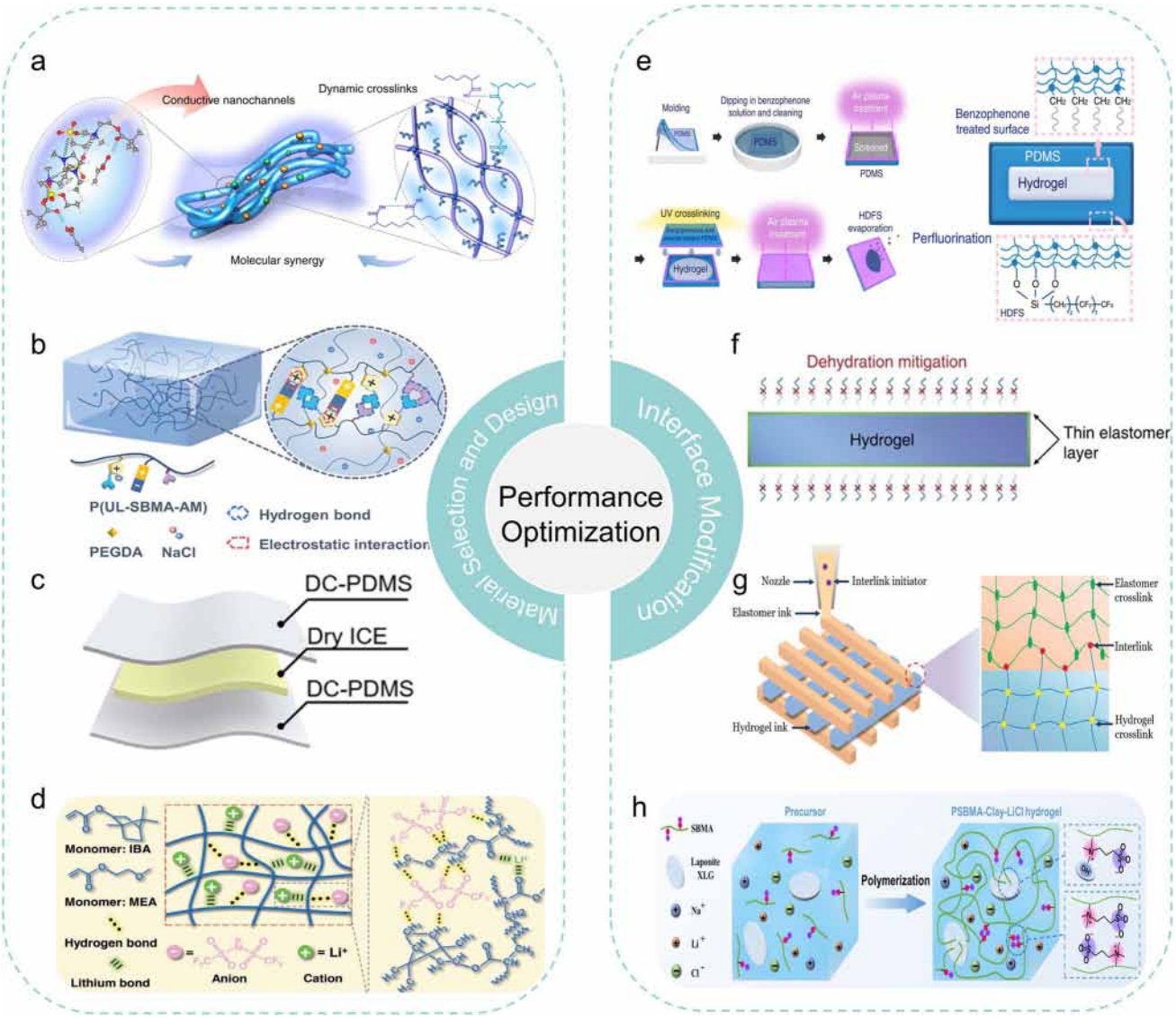

Fig. 7 Performance optimization of ionic receptors. Material selection and design: (a) the schematic diagram of a strategy for using ionic liquids that can form hydrogen bonds with polymer chains. Reproduced from ref. 123 with permission from the Author(s), copyright 2019. (b) The new hydrogel system based on an ionic liquid imidazolium salt with a ureido backbone (UL) to enhance mechanical properties and water retention. Reproduced from ref. 112 with permission from Wiley-VCH, copyright 2024. (c) Avoiding liquid leakage by using dry ion conductive elastomers (ICE). Reproduced from ref. 124 with permission from Wiley-VCH, copyright 2021. (d) Molecular design schematic of liquid-free ICE consisting of a copolymer network carrying lithium cations and related anions through lithium bonds and hydrogen bonds. Reproduced from ref. 125 with permission from Wiley-VCH, copyright 2021. Interface modification: (e) the robust interfaces between PDMS and hydrogel based on the chemical anchoring of benzophenone-treated (hexadecafluoro-1,1,2,2-tetrahydrodecyl)trichlorosilane (HDFS) coating. Reproduced from ref. 126 with permission from the Author(s), copyright 2018. (f) The skin-inspired hydrogel–elastomer mixture with a robust interface and functional microstructure. Reproduced from ref. 127 with permission from the Author(s), copyright 2016. (g) A method for printing the integrated structure of hydrogel and elastomer in any order and having strong adhesion. Reproduced from ref. 128 with permission from Wiley-VCH, copyright 2019. (h) The environmentally adaptable multifunctional hydrogel with strong adhesion strength by *in situ* polymerization of polyzwitterions in the presence of inorganic nanoclays and lithium chloride. Reproduced from ref. 113 with permission from Elsevier, copyright 2022.

anchoring between hydrogels and elastomers *via* benzophenone treatment (Fig. 7e). Zhao *et al.*[127] used benzophenone to modify cured elastomer surfaces, forming covalent crosslinks in the elastomeric polymer network and integrating hydrogels and elastomers into structures with strong interfaces (Fig. 7f). Suo *et al.*[128] developed a method to print integrated hydrogel and elastomer structures in arbitrary sequences. By incorporating a crosslinking initiator into one of the inks, covalent bonds were formed between hydrogel and elastomer networks, achieving adhesion energy exceeding 5000 J m^{-2} (Fig. 7g). Chen *et al.*[113] addressed these challenges by designing a composite hydrogel incorporating polyzwitterions, which provide self-adhesion through ion–dipole and dipole–dipole interactions with various substrates. Additionally, LiCl, a key solute with high moisture capacity and low molar mass, was utilized to simultaneously enhance the hydrogel's antifreeze properties, water

retention, and thermal tolerance (Fig. 7h). These methods have partially alleviated issues such as liquid leakage and poor self-adhesion in ionic receptors. However, several challenges persist. Firstly, material selection and design are often tailored to specific substances, and the crosslinking reactions are typically irreversible. Once the crosslinked structure is established, the material's shape and properties become difficult to modify, complicating processing technology and increasing demands. Additionally, the complexity and sensitivity of the interface modification process present challenges in precisely controlling dopant proportions, making it difficult to ensure consistent quality and effectiveness. Therefore, more convenient and effective strategies must be explored in future research to further enhance the performance and broaden the application range of ionic conductors.

3 Tele-perception systems based on TENG

3.1 Multi-receptor skin

Traditional non-contact sensors based on TENGs have garnered significant attention due to their unique interactive capabilities and notable advancements in research and applications. However, challenges persist, particularly in terms of sensing range, as achieving long-distance detection often necessitates larger devices. Additionally, key technical hurdles related to sensitivity adjustment and threshold setting remain unresolved.[61] Traditional TENG sensors often face challenges in maintaining stable charge over time and rely on basic signal processing methods, limiting their adaptability to environmental changes and restricting practical applications. As

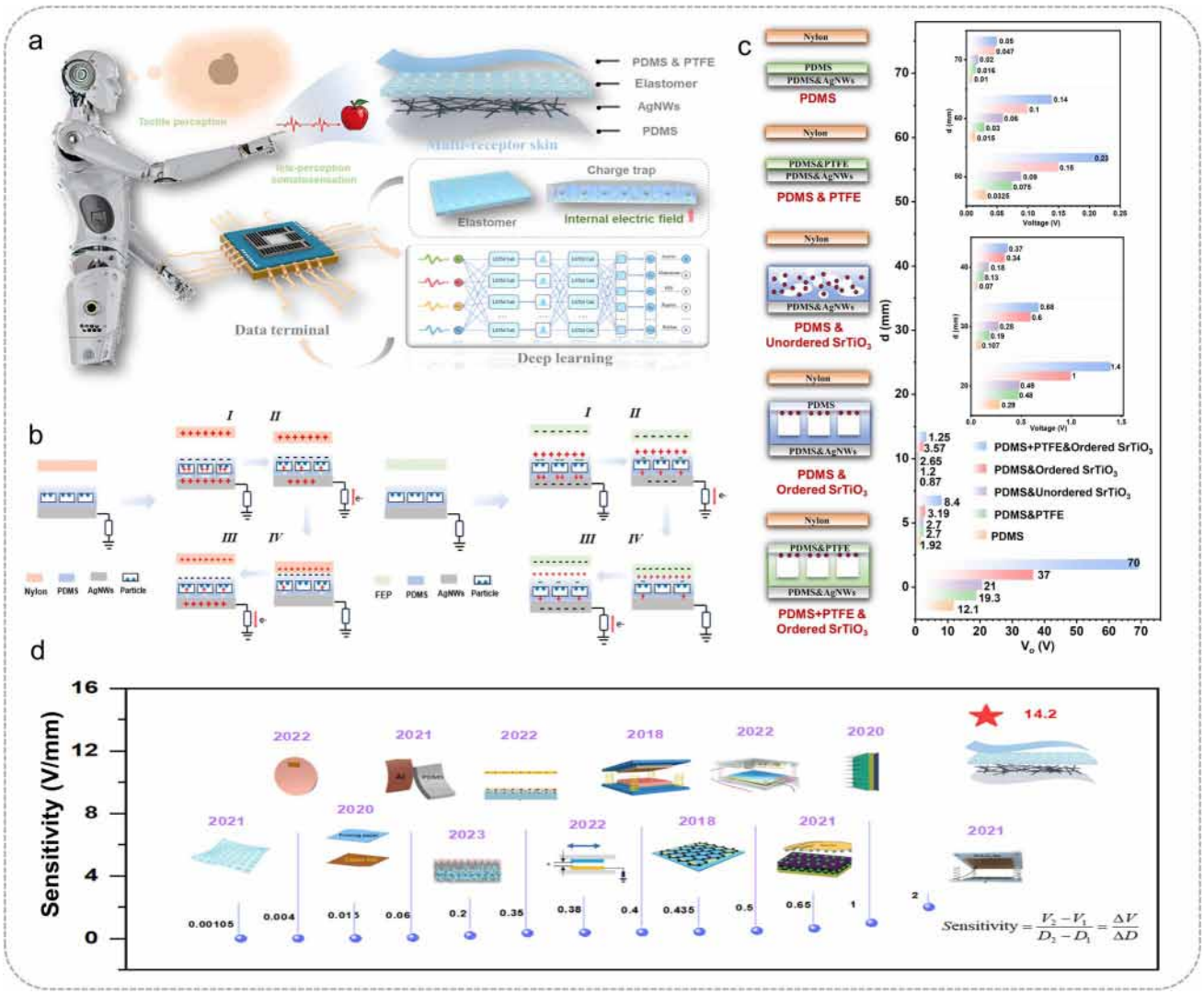

Fig. 8 Multi-receptor skin perception system. (a) Schematic diagram of intelligent perception system based on the multi-receptor skin and DL algorithms. (b) The working principle of the multi-receptor skin in response to proximity of positively or negatively charged objects. (c) Experimental verification of the effectiveness of inorganic non-metallic nanoparticles and microporous structure doping on signal acquisition enhancement. (d) The sensitivity comparison between the bionic inductor and some related inductors representative work. Reproduced from ref. 62 with permission from the American Association for the Advancement of Science, copyright 2024.

a result, optimizing the performance of traditional non-contact sensors, with a focus on developing technologies for efficient long-range detection, has become a central priority in this field. Recent research by Wei *et al.*[62] first introduced the concept of tele-perception, establishing a novel paradigm for remote sensing that redefines the possibilities of human perception and interaction. Compared to traditional non-contact sensors, tele-perception technology significantly increases the local electric field strength by integrating enhanced charge-trapping strategy combined with advanced structural design, thereby enhancing electrostatic charge retention. Moreover, tele-perception technology exhibits superior sensing performance by integrating advanced DL algorithms. This integration enables the realization of accurate dynamic detection, which is generally lacking in traditional TENG sensors. In material design, the enhanced electrostatic charge-trapping through structured doping of inorganic non-metallic nanoparticles (SiO_2, TiO_2, $BaTiO_3$ and $SrTiO_3$) was proposed. Nanoparticles with high dielectric constants exhibited superior electron capture efficiency, while non-metallic inorganic materials with non-centrosymmetric crystal structures exhibited polarization effects under external fields. This combination effectively prevented charge escape and enhanced sensing performance. In structural engineering, a bionic multi-receptor electronic skin for integrated tele-perception and tactile sensing was designed, as shown in Fig. 8a. Operating in single-electrode mode, it combined the principles of triboelectricity and electrostatic induction to achieve highly efficient, adaptive sensing capabilities. A crucial component of this system was the polarization-induced charge trap mechanism, where inorganic nanoparticles were orderly embedded within the elastomer's microporous structure. These nanoparticles interacted with pore surfaces to redistribute charges, forming charge traps that enhance the local electric field and optimize signal output. In the pre-charged state, doping the elastomer with inorganic nanoparticles induced dielectric polarization. When a positively charged nylon film approached, the polarization diminished, causing charge to flow through the circuit, while dielectric hysteresis ensured that residual polarization remained. This residual polarization acted as charge traps, significantly improving charge capture efficiency (Fig. 8b). It is demonstrated that signal acquisition was enhanced and voltage output was optimized by doping inorganic nanoparticles into microporous structures, as shown in Fig. 8c. In device optimization, an intelligent sensing system that integrated multi-receptor skin with DL algorithms was incorporated. The system's design allowed for seamless interaction with its environment, ensuring both high sensitivity and accuracy in detecting non-contact stimuli. A breakthrough sensitivity record of 142 V cm^{-1} was achieved through advancements in bionic inductor designs, as illustrated in Fig. 8d, marking a significant leap in tele-perception sensing capabilities.

3.2 Enhanced charge-trapping strategy for tele-perception

Wei *et al.*'s research represented a significant milestone in advancing sensing technology, shifting from traditional non-contact sensors to systems capable of extended sensing ranges, thus laying a robust foundation for the evolution of tele-perception.[62] However, fully unlocking the potential of tele-perception demands multi-level optimization, particularly in enhancing charge-trapping capabilities. Despite notable progress in boosting triboelectric charge density, challenges remain, especially due to charge dissipation processes such as neutralization by atmospheric water molecules.[129] To meet the high-performance demands of tele-perception, developing effective strategies to mitigate charge loss is crucial. This section delves into strategies aimed at improving charge-trapping efficiency, with a focus on chemical modification, the incorporation of interface layers, and nanoparticle doping. These approaches improve the sensing range, overall efficiency and reliability of the tele-perception system by enhancing charge retention and stability, which offer a theoretical framework for addressing current limitations and enabling future breakthroughs in the field.

3.2.1 Chemical modification. Chemical modification aims to enhance charge retention by facilitating the selective migration of induced ions, thereby suppressing charge dissipation, and by constructing deep trap structures to improve charge stability. Key approaches include free radical anion transfer, acid-ion complexation, functional group grafting, quenching polarization (QP), and molecular structure regulation. These strategies are critical for mitigating charge loss, stabilizing the electric field, and optimizing device output performance, addressing the fundamental challenges associated with charge dissipation in advanced applications.

Free radical anion transfer serves as a direct and efficient mechanism for selective migration, compensating for charge loss to the surrounding environment by facilitating the movement of free radical ions. It enhances charge stability and ensures the effective retention of charge within the system. Chen *et al.*[130] employed naphthalene radical anion as a wet chemical treatment agent for polytetrafluoroethylene (PTFE), producing ionized PTFE (I-PTFE) with a high concentration of free radical ions. These free radical ions compensated for charge escape *via* selective transfer induced by mechanical force, achieving ultra-high charge density (Fig. 9a). Building on this, they proposed the acid-ion complexation method to fabricate positively charged triboelectric materials with enhanced charge retention. This approach leverages the formation of acid-ion complexes to increase the activation energy required to release stored charges, thereby improving charge stability.[131] It can also induce selective anion migration to compensate for the escape of polarized charges, achieving a charge density of 596 μC m^{-2} and a charge retention rate of 49.7% (Fig. 9b). The primary approaches for creating deep trap structures include functional group grafting, which involves attaching specific functional groups to the material surface to enhance charge trapping; quenching polarization (QP), which generates ultrahigh and long-lasting triboelectric charge density through molecular deformation and deep trapping; and molecular structure regulation, which directly tailors the material's structure to form deep traps, thereby improving charge stability. For example, Wang *et al.*[132] introduced sulfonic

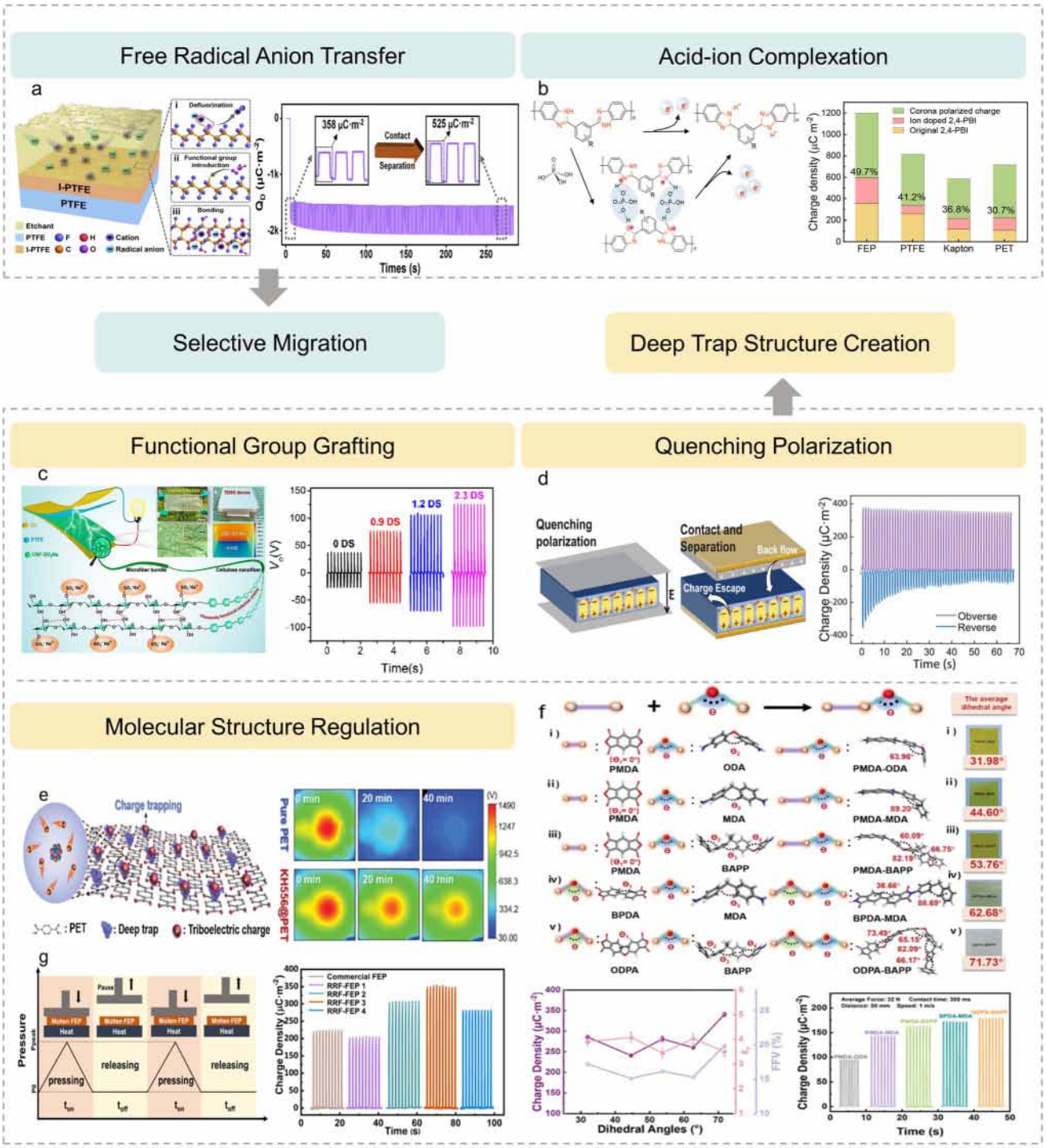

Fig. 9 Selective migration: (a) the method to achieve ultra-high charge density in the open air by using free radical anion transfer as a compensation for charge escape. Reproduced from ref. 130 with permission from Elsevier, copyright 2023. (b) A method to suppress charge escape in the open air by acid-ion complexation. Reproduced from ref. 131 with permission from American Chemical Society, copyright 2024. Deep trap structure creation: (c) ultra-high electrical output device with sulfonated cellulose nanofibers as a positively charged tribolayer. Reproduced from ref. 132 with permission from American Chemical Society, copyright 2022. (d) A method to induce a large number of interface deep traps by QP. Reproduced from ref. 133 with permission from Wiley-VCH, copyright 2023. Molecular structure regulation: (e) a strategy of introducing self-assembled molecules with large energy gaps to form deep carrier traps. Reproduced from ref. 134 with permission from Wiley-VCH, copyright 2024. (f) The strategy of dihedral angle adjustment in molecular engineering to prevent charge escape. Reproduced from ref. 137 with permission from Wiley-VCH, copyright 2024. (g) A strategy to effectively tune the molecular structure of triboelectric polymers by repeated rheological forging (RRF) process. Reproduced from ref. 138 with permission from the Author(s), copyright 2022.

acid groups into cellulose nanofibers (CNF) to produce CNF–SO_3Na. Sulfonic acid functional groups with high electrostatic potential and uniform distribution acted as deep traps, enhancing the triboelectric charge capture ability of modified CNF and increasing the electrical output performance (Fig. 9c). Qu *et al.*[133] increased the number of interfaces between crystalline and amorphous regions on weak polar polymer and generated numerous interface deep traps for charge storage by QP. The sensor prepared using this method achieved a maximum charge density of 391 μC m^{-2}, 200% higher than that achieved by conventional polarization methods (Fig. 9d). In addition, self-assembled molecules with large energy gaps onto commercial PET fibers was introduced to create deep carrier traps.[134] Manipulating the trap distribution within the triboelectric layer reduces triboelectric charge dissipation, thereby enhancing the electrical output (Fig. 9e). In polymers, the dihedral angle between adjacent conjugated planes (conjugated dihedral angle) is a crucial factor in modulating molecular structure, thereby affecting trap distribution and ultimately determining performance.[135,136] Variations in this angle can significantly affect the electronic properties of the polymer, including band structure and charge transfer behavior. Recognizing this, Li *et al.*[137] systematically tailored the conjugated dihedral angle in polyimide (PI) chains by incorporating different monomers into the polymer backbone. By increasing the dihedral angle, they weakened the conjugation between molecular chains, thereby expanding the energy gap between molecular orbitals and suppressing the formation of charge transfer complexes (CTCs). This approach highlights the importance of controlling molecular geometry to optimize polymer performance. Chen *et al.*[138] effectively modified the molecular structure of triboelectric polymers by RRF process, including molecular orientation, crystallinity and dielectric constant. In ethylene propylene fluoride (FEP) films with high crystallinity, numerous deep traps formed at the interface between microcrystalline and amorphous regions, enhancing charge storage. The intrinsic surface charge density was 1.46 times higher than the previously reported record. Additionally, the sensor's output charge density, achieved using a 30 μm thick thin film, reached 352 μC m^{-2} (Fig. 9g). Collectively, these chemical modification techniques offer valuable insights for optimizing charge retention, thereby enhancing the long-term performance and reliability of tele-perception systems.

3.2.2 Interface layer incorporation. Additionally, the incorporation of interface layer serves as an effective strategy to maintain triboelectric charge density and extend the surface charge decay time.[139,140] This approach involves three key aspects. First, the electron blocking layer or charge storage layer is designed to create a space charge region and provide electron capture sites for charge storage, establishing a foundation to enhance output performance. Second, the electron transmission layer facilitates the transfer of surface electrons to the triboelectric layer while minimizing electron diffusion, ensuring efficient charge transmission and utilization. Lastly, high permittivity materials are incorporated to enhance polarization effects, increasing the number of induced charges and ultimately improving output performance. Together, these interface layer strategies provide a critical solution to sustaining charge retention and enhancing the overall efficiency of non-contact sensing systems.[141]

In terms of the electron blocking layer or charge storage layer, Lai *et al.*[78] developed graphitic carbonized textiles to achieve the long-term retention of triboelectric charges. Sensors constructed with this approach exhibited excellent output performance during non-contact operations over various separation distances, maintaining triboelectric charges for up to 5000 minutes (Fig. 10a). Wen *et al.*[142] integrated a solution-processed high-permittivity electron blocking layer composed of LaZrO into the device to form an energy barrier (ΔE > 1.3 eV) between the transparent indium tin oxide (ITO) and PDMS, blocking electron transfer to the bottom electrode to reduce the surface potential decline rate of PDMS and extend the charge decay time by approximately 3.1 times (Fig. 10b). Additionally, a MoO_3 electron blocking layer was introduced between the ITO electrode and the fluorinated ethylene propylene (FEP) polymer triboelectric layer.[143] This layer effectively mitigates charge shielding effects at the interface, polarizes the FEP layer, and consequently improves and stabilizes charge trapping (Fig. 10c). For the electron transmission layer, Tang *et al.*[144] enhanced charge storage by designing rhombus-shaped all-inorganic perovskite nanoarrays functioned as a conductive transmission layer sandwiched between the triboelectric layer and an inserted dielectric layer, facilitating the transfer of surface charges to deeper regions, thereby enabling enhanced charge storage (Fig. 10d). In terms of the high permittivity materials incorporation, Wang *et al.*[145] introduced a dual-dielectric layer that effectively suppressed dielectric charge leakage, enhancing the output performance to 2200 μC m^{-2} (Fig. 10e). Similarly, LIG doped with MoS_2 was integrated to achieve a fourfold increase in surface potential.[69] The synergistic interaction between MoS_2 and LIG enhanced interlayer dielectric properties and polarization, ultimately improving the output performance (Fig. 10f).

3.2.3 Nanoparticle doping. Nanoparticle doping, a simple and cost-effective preparation process, is employed to improve the surface charge density of dielectric layer to enhance the performance, without complex system design and harsh working environment requirements.[146–148] This approach involves four key aspects. Integrating metal nanoparticles with strong electron trapping or storage capabilities into triboelectric materials provides an effective strategy for maintaining bulk charges and enhancing overall charge density. They improves charge retention while preserves device flexibility by capturing charges and inhibiting charge flow from the dielectric layer to direct recombination. In contrast, metal oxide nanoparticles improve dielectric properties by acting as charge storage layers, stabilizing charge separation and ensuring charge retention. Non-metallic inorganic nanoparticles create abundant trap sites, significantly reducing charge dissipation and enhancing system stability. Ferroelectric nanoparticles enhance polarization effects, further improving the material's charge retention capability and consolidating charge storage. The synergistic interaction of these nanoparticles optimizes the charge-related

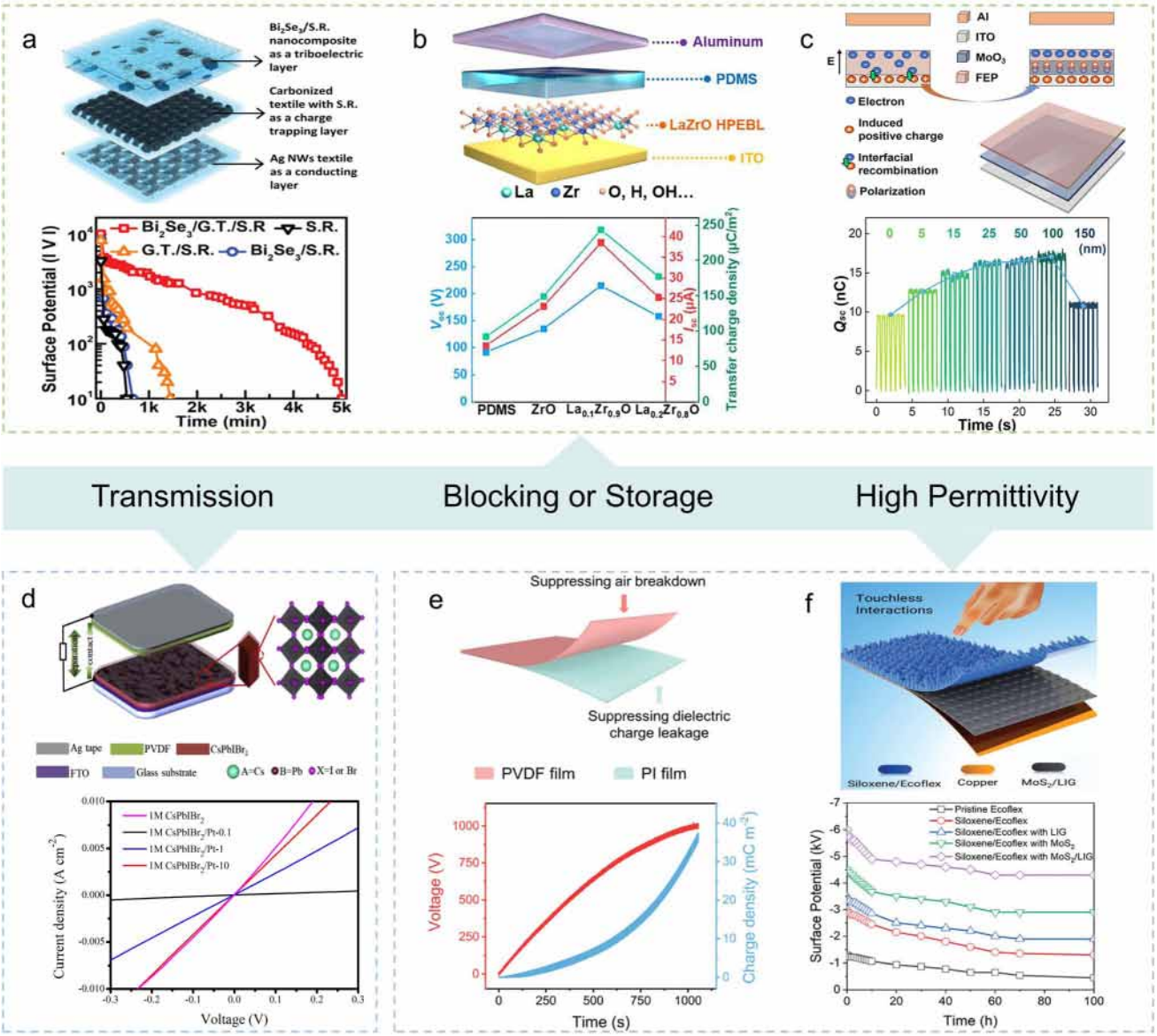

Fig. 10 Methods of interface layer incorporation. Electron blocking layer or charge storage layer: (a) method for extending the triboelectric charge retention time by using graphitic carbonized textiles as a charge storage layer. Reproduced from ref. 78 with permission from Wiley-VCH, copyright 2024. (b) A method of embedding a solution-processed high-permittivity electron blocking layer of lanthanum zirconium oxides (LaZrO) to prevent the transmission of electrons to the bottom electrode. Reproduced from ref. 142 with permission from Elsevier, copyright 2022. (c) A method to increase the surface charge density by adding a MoO_3 as electron blocking layer with high dielectric constant and wide band gap. Reproduced from ref. 143 with permission from American Chemical Society, copyright 2022. Electron transmission layer: (d) a method to enhance and store charge by customizing a diamond-shaped all-inorganic perovskite nanoarray as a electron transmission layer. Reproduced from ref. 144 with permission from Elsevier, copyright 2020. High permittivity materials incorporation: (e) a strategy to suppress the charge decay of high surface charge density device by using a double dielectric layer. Reproduced from ref. 145 with permission from Wiley-VCH, copyright 2023. (f) A method to enhance dielectric properties and polarization by introducing MoS_2/laser-induced graphene (LIG). Reproduced from ref. 69 with permission from Wiley-VCH, copyright 2022.

properties of triboelectric materials, enabling broader applications in advanced energy and sensing systems.

For metal nanoparticles, Meng *et al.*[149] designed a Co–NPC/Ecoflex composite layer with a microstructured square-loop surface to develop a single-electrode mode non-contact sensor, layering over a dielectric copper calcium titanate/Ecoflex nanocomposite with an ultra-high dielectric constant. The fine Co nanoparticles with high specific surface area uniformly disperse in the NPC matrix, which benefits in capturing generated charges and stabilize output energy. Through extensive optimization of material selection, component composition and structural design, the sensor, with an effective electrode area of 6.25 cm^2, generated a high output voltage of 29 V at a 1 cm distance and detected motion up to 6 m away (Fig. 11a). For metal oxide nanoparticles, Zhai *et al.*[150] improved the dielectric constant by doping BTO nanoparticles

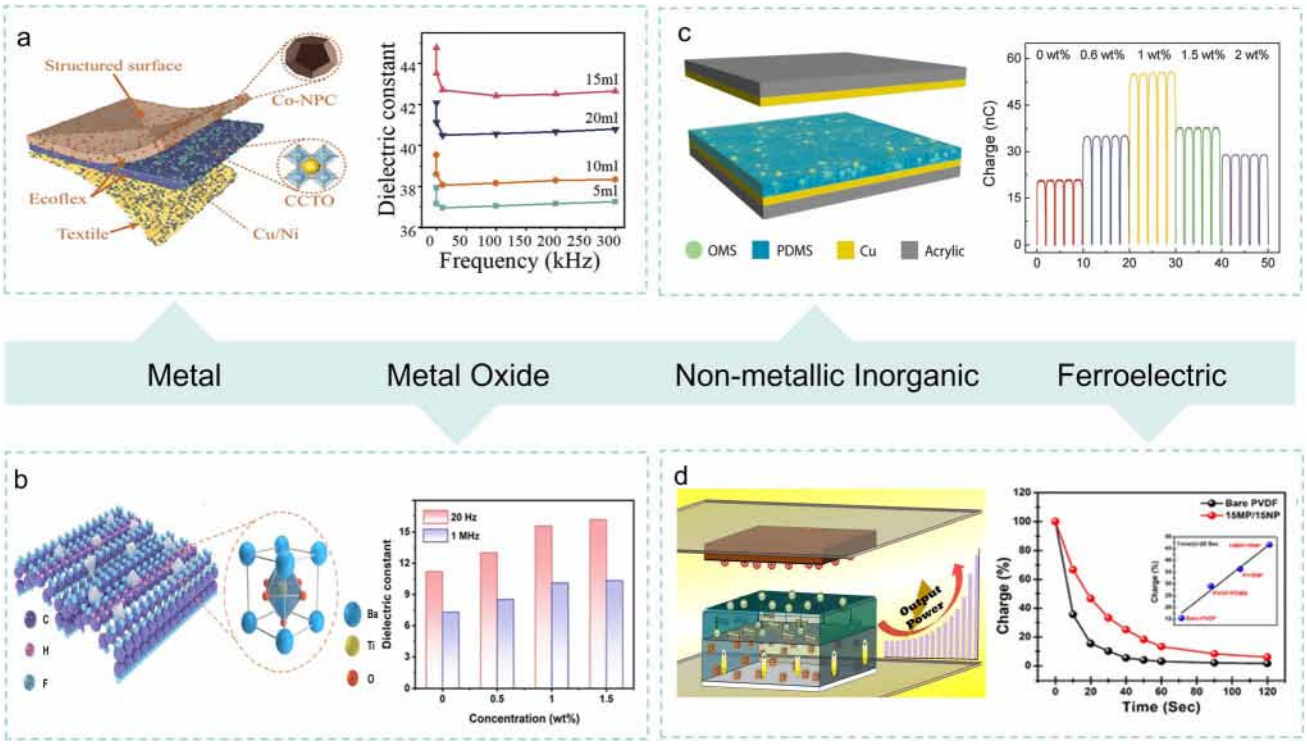

Fig. 11 Methods of nanoparticles doping. (a) A triboelectric Co–NPC/Ecoflex nanocomposite layer with a microstructured square-ring surface was constructed by using functional nanofillers, extending the non-contact sensing capability of the sensor to a few meters for the first time. Reproduced from ref. 149 with permission from Elsevier, copyright 2024. (b) A method to further enhance the triboelectric properties by doping $BaTiO_3$ (BTO) nanoparticles with high dielectric constant. Reproduced from ref. 150 with permission from Elsevier, copyright 2024. (c) A strategy to enhance the output performance by adding ordered mesoporous SiO_2 nanoparticles as charge storage sites. Reproduced from ref. 151 with permission from Elsevier, copyright 2023. (d) A method of introducing $NaNbO_3$ ferroelectric nanoparticles into the PDMS matrix to enhance internal polarization and increase trap sites, thereby maintaining the generated surface charge for a longer time. Reproduced from ref. 152 with permission from American Chemical Society, copyright 2024.

and further enhanced the output with an external charge pump module, achieving a total transferred charge density of 3500 μC m^{-2} using an external capacitor with a capacitance of 20 nF (Fig. 11b). And for non-metallic inorganic nanoparticles, orderly mesoporous SiO_2 nanoparticles (OMS) were utilized as charge storage sites to improve the output performance.[151] The enhancement effect of OMS nanoparticles on output demonstrated a linear relationship with their specific surface area. When the concentration of OMS nanoparticles increased to 1 wt%, the transferred charge rose sharply from 21 nC to 60 nC due to the additional bulk charges stored by OMS nanoparticles. Furthermore, OMS–PDMS exhibited superior charge retention capability after contact–separation motions ceased, with its voltage remaining stable for an extended period, while the voltage of pure PDMS rapidly dropped to near zero. The OMS–PDMS device achieved an instantaneous output power density of 5.26 W m^{-2}, representing a 25-fold improvement (Fig. 11c). In terms of ferroelectric nanoparticles, Khare *et al.*[152] proposed a sensor with a bilayer negatively charged structure. Incorporating ferroelectric $NaNbO_3$ nanoparticles into the PDMS bottom layer enhanced internal polarization and created additional trap sites, enabling longer retention of generated surface charges. The synergistic interaction between these two layers significantly enhanced the overall performance (Fig. 11d).

Although these approaches have not yet been widely adopted in non-contact sensing devices, they offer highly effective solutions for enhancing charge-trapping capabilities. Improving charge retention is crucial for achieving high-performance tele-perception. As related technologies continue to advance and optimize, these methods are expected to significantly boost tele-perception performance. Potential advancements may include enhanced sensing sensitivity, extended sensing range, and improved signal output stability, driving technological upgrades and innovative tele-perception applications across diverse fields, such as environmental monitoring, intelligent security systems, and industrial automation.

3.3 Algorithm enhancement strategy

The enhancement of charge-trapping capabilities is fundamentally achieved through strategic material selection and design, constituting the hardware framework. Equally pivotal, however, is the software dimension, where advancements in algorithm integration and optimization are indispensable for driving further enhancements in system performance. Integrating sensors with advanced data processing systems, akin to the synergy between receptors and nerves in the peripheral nervous system (PNS), substantially enhances system

responsiveness in dynamic and complex environments.[153] This integration improves sensitivity, accuracy, and facilitates real-time data processing and decision making, enabling effective resolution of intricate sensing tasks. In terms of traditional non-contact sensors and tele-perception technology based on TENG, machine learning (ML), as an emerging technology for extracting nuances and processing multi-channel signals, provides unique advantages for efficient analysis and processing of sensing signals.[154] Currently, widely used ML algorithm models in TENGs include support vector machine (SVM),[155] random forest (RF),[156] K-nearest neighbor (KNN),[157] CNN,[158] recurrent neural network (RNN),[159] artificial neural network (ANN),[160] principal component analysis (PCA),[161] decision tree (DT),[162] multi-layer perceptron (MLP),[163] and extreme gradient boosting (XGB),[164] *etc.* These techniques effectively tackle the challenges of complex pattern recognition and efficient data processing by leveraging adaptive modeling, enhanced signal processing, and improved prediction accuracy. However, it is undeniable that the application of ML is highly dependent on the dataset, and it is unrealistic to associate a single algorithm with a specific application field. Bionic iontronics provide the possibility of developing highly efficient, brain-like neuro-iontronics for in-sensor computing devices.[165] Accordingly, this section delves into algorithmic enhancement strategies, including multi-data fusion techniques, neuromorphic sensing architecture designs, and adaptive learning rules, aiming to establish theoretical foundations and technical pathways for advancing the overall performance of tele-perception systems.

Multi-data fusion techniques focus on achieving consistent interpretation of the observed environment by leveraging multi-level and spatially diverse information through complementary and optimized processing, significantly improving environmental perception accuracy and reliability. Analogous to cognitive functions in the human brain, cross-modal sensory information interactions enable learning frameworks to make more precise and continuous predictions about stimulus

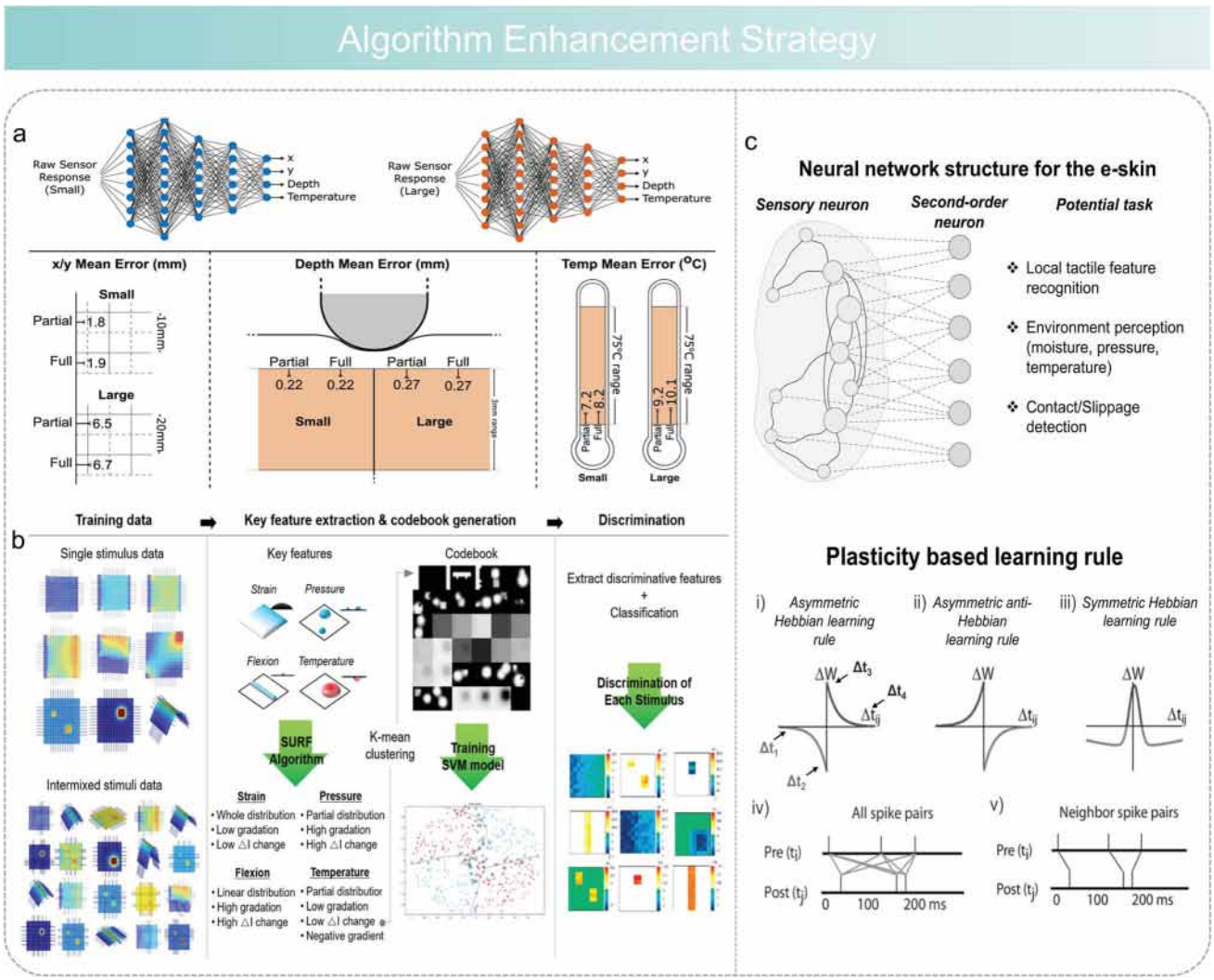

Fig. 12 (a) Response input tactile stimulation prediction based on learning algorithm. Reproduced from ref. 166 with permission from Wiley-VCH, copyright 2023. (b) A schematic diagram using the bag-of-words (BoW) algorithm to distinguish mixed stimuli. Reproduced from ref. 167 with permission from Wiley-VCH, copyright 2020. (c) The neural network structure and adaptive learning rules for the proposed computational e-skin. Reproduced from ref. 168 with permission from the American Association for the Advancement of Science, copyright 2022.

location, depth, and temperature. For example, Clemens *et al.*[166] achieved biomimetic sensory capabilities by integrating piezoresistive sensing elements with learning algorithms, enabling continuous perception of light touch, depth, and temperature (Fig. 12a). Similarly, Mo *et al.*[167] developed a highly stretchable cross-reactive sensor matrix with artificial perception capabilities that enables the detection, classification, and differentiation of various tactile and thermal stimuli using machine learning. Specifically, multimodal sensing was achieved through the learning algorithm based on the bag-of-words (BoW) model, which identified distinct 2D image patterns generated by mixed tactile and thermal stimuli, enabling differentiation of each stimulus. This approach offered a versatile pathway to simplify e-skin systems, reduce architectural complexity and enhance adaptability to diverse environments, surpassing the limitations of traditional "lock-and-key" methods (Fig. 12b). Additionally, neuromorphic sensing building blocks exhibit significant potential in intelligent sensing, emphasizing the mimicry of neural sensing and data processing mechanisms observed in biological systems to enhance sensory performance. For instance, Dahiya *et al.*[168] proposed a neural architecture for computational e-skin, comprising a sensory neuron layer and a cuneate neuron layer interconnected by synapses. Analogous to mechanoreceptors with diverse receptive fields, stimulation of a single neuron influenced its surrounding neurons. This mechanism mapped incoming tactile signals into a higher-dimensional space in the first layer for processing, and then fed the output into the second layer for further processing, thereby supporting robots to perform diverse tasks, including localized tactile feature recognition and contact/sliding detection. Notably, the plasticity-based learning rule (STDP) proved particularly suitable for hardware applications, especially in synaptic devices. Under this rule, synaptic weights were determined only by the time correlation between paired spikes from the pre- and post-neurons, and operated according to various pairing schemes, including "nearest-neighbor takes all", "nearest-neighbor takes more", or "all-spike pairs count equally", providing promising avenues for further enhancing the sensory capabilities of e-skin.

4 Application scenarios

4.1 Applications of traditional non-contact sensors

Non-contact sensors represent a significant breakthrough in science and technology, functioning as a crucial link for the advancement of intelligent interaction, facilitating innovative interaction paradigms and demonstrating substantial potential for diverse applications. This section reviews recent advancements on traditional non-contact sensors in various application areas, including HMI, intelligent monitoring and machine learning assistant systems.

In HMI, non-contact sensors present a novel interaction mode. Compared to traditional methods relying on physical buttons and touchscreens, they enable more natural and seamless interactions, particularly excelling in humanoid robots, touch line screens and AR/VR systems. In humanoid robot applications, Chen *et al.*[77] utilized BAA sensors to successfully implement hand-avoidance functionality, as shown in Fig. 13a. Pu *et al.*[70] developed a virtual distance alarm robot interface with indicator lights controlled by calibrated threshold voltage, displaying corresponding color changes based on varying distances (Fig. 13b). Similarly, Cao *et al.*[75] designed humanoid robots equipped with distance sensors capable of exhibiting human-like perceptual behavior (Fig. 13c). For touch line screens, non-contact sensors provide broad application prospects, including remote password verification,[61] contactless control panels to reduce virus risk[70] and keyless electronic door lock systems.[74] In the AR/VR field, innovative breakthroughs continue to emerge. One example is a non-contact keyboard powered by a resonant triboelectric nanogenerator (R-TENG), comprising a self-powered transmission unit and a non-contact coupling unit[169] (Fig. 13g). Another notable example is the intelligent, contactless wearable keyboard system developed by Park *et al.*[59] When users operated the keyboard with their fingers at a specific distance, the system produced text such as "ASER" (Fig. 13h). Additionally, Yuce *et al.*[170] developed a comprehensive HMI system for cursor control, leveraging a self-powered eye motion sensor based on triboelectric interaction and near-field electrostatic induction, significantly improving interaction flexibility in wearable assistive technologies (Fig. 13i).

In intelligent monitoring, non-contact sensors facilitate real-time monitoring of human physiological parameters, behaviors and industrial conditions, providing a robust foundation for medical diagnosis, health management and industrial automation. For intelligent healthcare, non-contact monitoring of vital signs such as breathing and heartbeat ensures continuous, reliable data collection and aids in the timely detection of potential health issues.[171] In daily care, the device autonomously detects and differentiates complex human movements without human intervention,[172] facilitating multi-site, multi-dimensional motion monitoring[65] and providing essential support for rehabilitation *via* postoperative gait analysis.[173] During the COVID-19 pandemic, the device was adapted as a non-contact gesture recognition system to enable robot-assisted throat swab collection.[174] In addition, the advancements of intelligent industry are closely linked to non-contact devices. A non-contact sensing system for robot collision avoidance is illustrated Fig. 14f, with sensors installed at the front and rear of the vehicle to detect and avoid obstacles.[73] Furthermore, as shown in Fig. 14g, the system can serve as a highly sensitive and reliable speed sensor for commercial vehicles.[72] A limit alarm device[173] that utilized a non-contact motion vector sensor with multi-channel signal acquisition capabilities was shown in Fig. 14h. During operation, the device prevented collisions between the positioning block and the limit block as the positioning block approached the alarm position, thereby prolonging the machine's service life. Additionally, as shown in Fig. 14i, non-contact sensors are applicable in diverse motion environments, including reverse engineering, grasping detection, and intelligent control.[173] Notably, these sensors exhibit high effectiveness in non-contact hand sanitizer devices[69] (Fig. 14j). In industrial health management and public spaces with high personnel traffic,

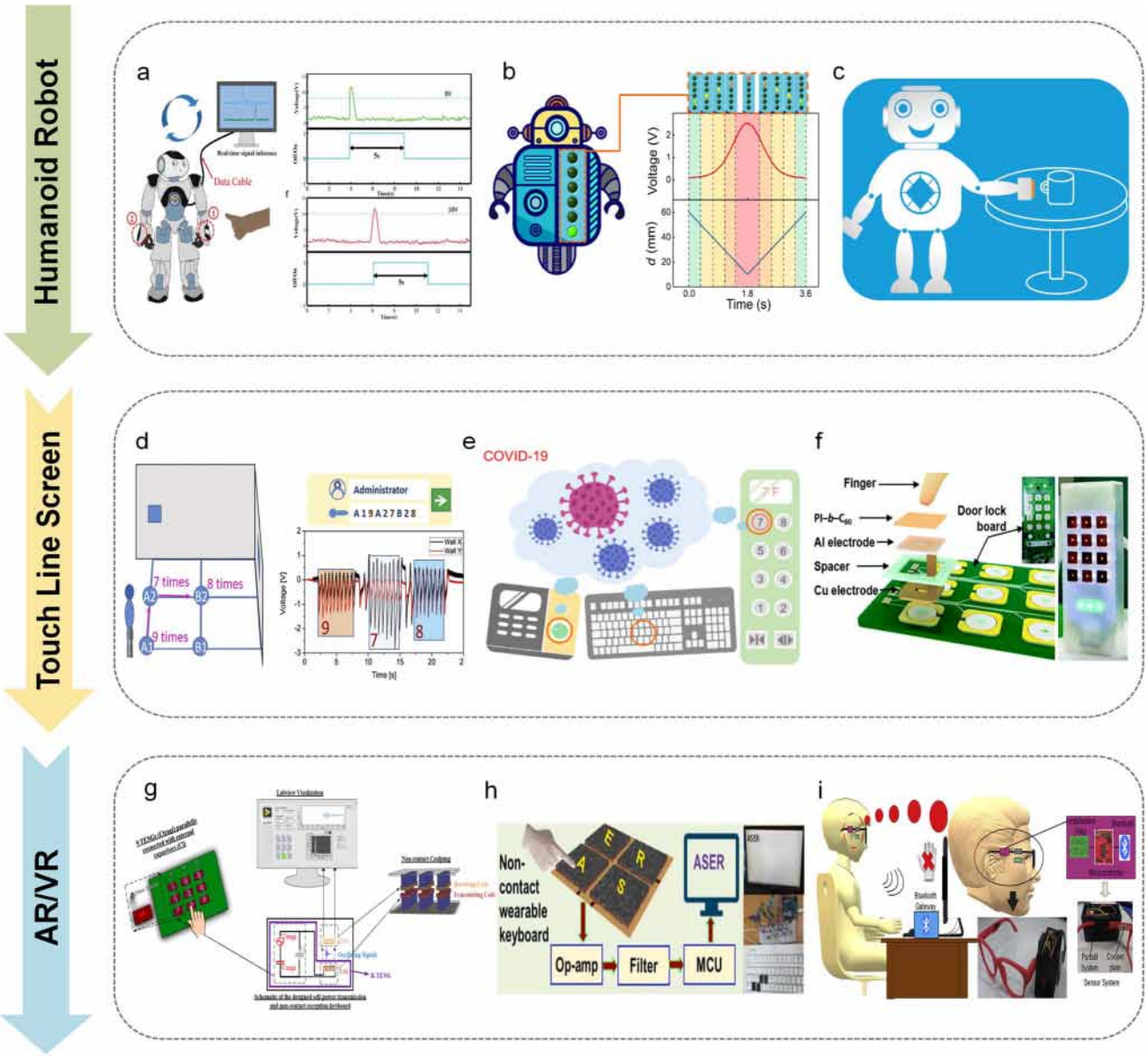

Fig. 13 Applications of traditional non-contact sensors in HMI. (a) Interactive interface for robot hand control. Reproduced from ref. 77 with permission from Wiley-VCH, copyright 2019. (b) Virtual distance alarm robot based on distance sensing inductor. Reproduced from ref. 70 with permission from the American Association for the Advancement of Science, copyright 2022. (c) Perceptual behavior of humanoid robot based on distance sensor. Reproduced from ref. 75 with permission from American Chemical Society, copyright 2020. (d) Non-contact device for password verification. Reproduced from ref. 61 with permission from Elsevier, copyright 2019. (e) Touchless control panel for preventing virus risk. Reproduced from ref. 70 with permission from the American Association for the Advancement of Science, copyright 2022. (f) Non-contact sensing for keyless electronic door lock systems. Reproduced from ref. 74 with permission from Royal Society of Chemistry, copyright 2021. (g) Non-contact receiving keyboard based on R-TENG. Reproduced from ref. 169 with permission from Elsevier, copyright 2018. (h) Wearable keyboard based on CNM-TENG. Reproduced from ref. 59 with permission from Elsevier, copyright 2022. (i) Comprehensive HMI system for cursor control. Reproduced from ref. 170 with permission from Elsevier, copyright 2020.

they detect hand proximity to trigger automatic hand sanitizer dispensers, preventing cross-contamination issues associated with traditional shared devices, enhancing hygiene standards, and highlighting the critical role of non-contact sensors in smart industry applications. Furthermore, non-contact devices demonstrate significant potential in hydrological measurement and geological resource exploration[175] (Fig. 14k). Moreover, non-contact devices are widely used for position monitoring. Single-electrode TENG (STENG) sensors detect the charge type of charged objects, while freestanding TENG (FTENG) sensors identify their motion direction. Based on this principle, STENG-based sensors were installed at the entrance of a complex space, and FTENG-based sensors were placed at various positions within the space, enabling effectively monitoring of the moving direction and trajectory of charged objects,[176] as shown in Fig. 14l. Another sensor capable of identifying human motion

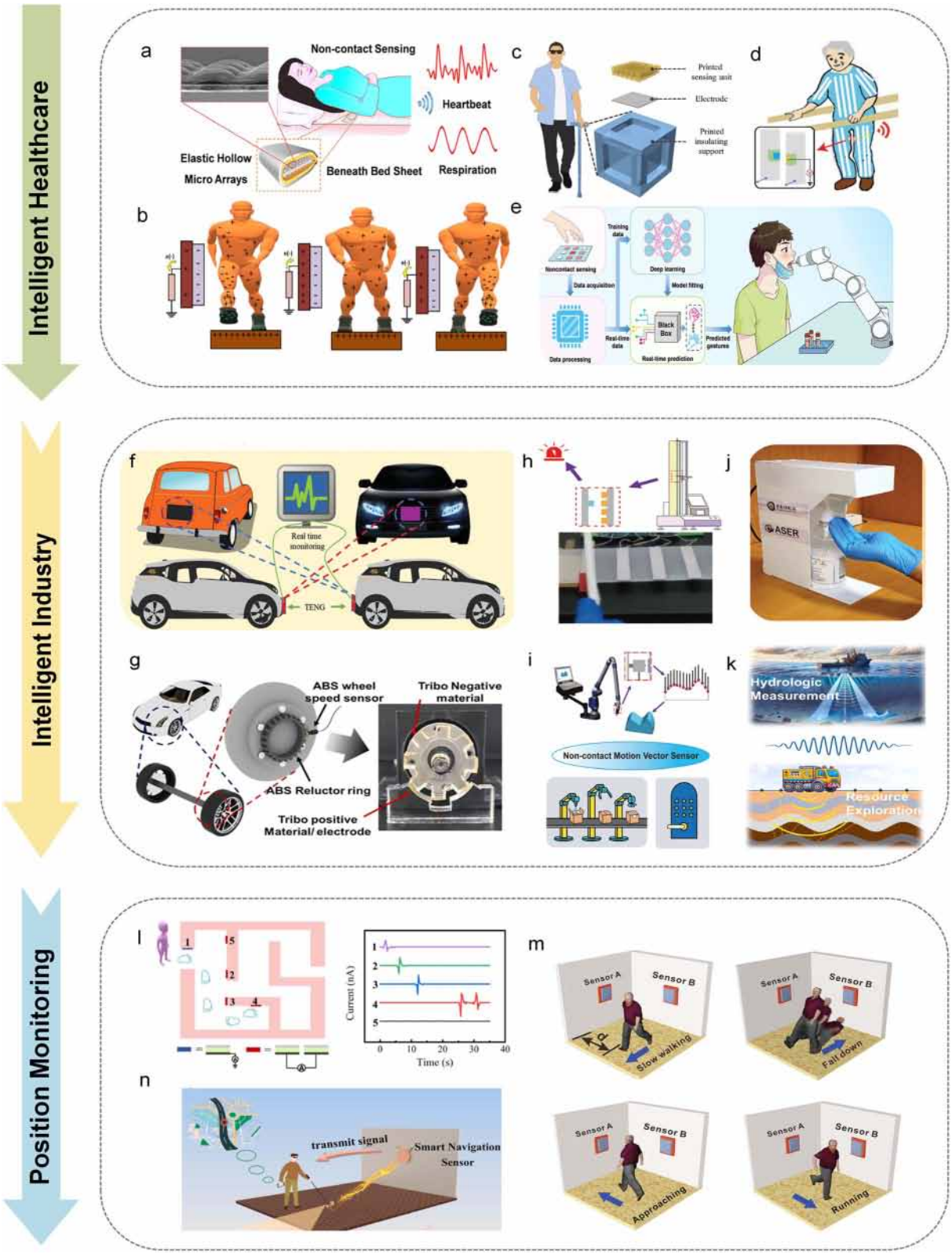

Fig. 14 Applications of traditional non-contact sensors in intelligent monitoring. (a) Non-contact heartbeat and respiration monitoring system. Reproduced from ref. 171 with permission from American Chemical Society, copyright 2018. (b) A non-contact sensing platform that can monitor and distinguish complex human movements. Reproduced from ref. 172 with permission from Elsevier, copyright 2021. (c) Non-contact multi-directional motion monitoring sensor based on 3D printing deep trap layered architecture. Reproduced from ref. 65 with permission from Elsevier, copyright 2022. (d) Non-contact sensor for gait monitoring of patients after surgery. Reproduced from ref. 173 with permission from Wiley-VCH, copyright 2022. (e) A non-contact gesture recognition system for controlling the robot to collect throat swabs. Reproduced from ref. 174 with permission from Wiley-VCH, copyright 2022. (f) A non-contact sensing system for obstacle prevention in robotic vehicles.

states and indoor positions, such as walking, falling, approaching and running is illustrated in Fig. 14m, making it valuable for assisting the blind and elderly.[71] Additionally, Peng *et al.*[177] designed a user-friendly intelligent navigation sensor for the visually impaired, enabling effective obstacle avoidance (Fig. 14n).

Integrating ML algorithms with non-contact sensors provides an innovative solution to the challenges of computing power and complex circuitry in high-resolution devices, enabling multifunctional capabilities with fewer sensors by leveraging efficient data analysis and processing and achieving more efficient interactions and intelligent response mechanisms.[179] This synergy enhances motion recognition accuracy and promotes the application and development of non-contact sensors in fields such as smart homes, health monitoring, and AR, assisting them to address user needs more effectively and providing intelligent, adaptive functions supported by continuously optimized data processing capabilities. Firstly, ML algorithms have significantly enhanced the accuracy of non-contact gesture recognition. To address the challenge of distinguishing similar voltage sequences, Yang *et al.*[180] utilized PCA to extract features from collected data, demonstrating clear divisibility in two-dimensional space. They employed six algorithms—KNN, SVM, RF, DT, MLP, and XGB—to train the gesture recognition model, achieving accuracies of 0.82, 0.92, 0.94, 0.94 and 0.98 for different gestures, demonstrating excellent performance (Fig. 15a). Using the KNN learning algorithm, Zhao *et al.*[113] successfully trained a model to classify data for non-contact digital recognition, achieving an 88% overall accuracy in identifying ten digits after 20 training cycles (Fig. 15b). Moreover, ML algorithms enhanced the accuracy of material shape recognition. Pu *et al.*[70] developed an artificial proximal somatosensory system for 3D recognition by inputting simulation results from an electric receptor matrix into a CNN, achieving a recognition accuracy of 97% after 75 training cycles (Fig. 15c). Wen *et al.*[181] integrated a CNN into an intelligent soft robot system and enhanced its performance through iterative optimization. After training on 270 original datasets, the robot system achieved 97% recognition accuracy. By accurately perceiving and describing the object's features, the soft robot deformed and grasped objects based on recognition results from multi-modal sensors (Fig. 15d). Furthermore, ML algorithms also enhance human motion pattern recognition. Different motion patterns, such as walking, running and jumping, generate distinct responses in non-contact sensors. Wan *et al.*[182] applied RF algorithms to train motion recognition models to extract and identify features from human motion signals, facilitating the development of multimodal integrated e-skin, demonstrating significant potential for diverse applications (Fig. 15e).

4.2 Applications of tele-perception systems

The proposal of tele-perception introduces a novel approach to expanding the innovative dimensions of human perception and cognition. In HMI scenarios, tele-perception exhibits more sensitive and stable response signals compared to traditional non-contact sensors. As illustrated in Fig. 16a, Wei *et al.*[62] proposed a pioneering tele-perception HMI scenario where a robot equipped with a bionic electroreceptor functioned as proximity sensor to detect human motion. Building on this, a virtual distance alert interface was developed, featuring dynamically switching indicators based on calibrated threshold voltages. These threshold adjustments accommodate targets with varying surface charges or materials. Furthermore, tele-perception in HMI was demonstrated through a robot utilizing bionic inductors to detect human electrical signals with threshold voltage configured using the LabVIEW software program, and when signals exceeded the threshold, the robot arm interacted with the individual. This application significantly enhances the potential of tele-perception in robotics and HMI.

ML algorithms further improved the system's ability to effectively interact with the real-world. As shown in Fig. 16b, a 3D tele-perception somatosensory system employed a CNN to efficiently identify and perceive the shapes and materials of various 3D objects while offering detailed 3D visualization. Using common indoor geometric configurations (humans, chairs, and tables) as test examples, the system achieved 100% recognition accuracy after only three training cycles, establishing a robust foundation for future practical applications. Additionally, the system utilized spectral data to learn the unique color features of various materials and associated them with corresponding material types through ML algorithms and DL models, enabling accurate material identification, even for distant or partially obscured objects. This technological advancement created more opportunities in intelligent robotics, autonomous vehicles and industrial manufacturing. The core value of tele-perception lies in its ability to extend human perception, offering a more intelligent perception method for machines and accelerating advancements in HMI, automatic control and related fields.

5 Conclusions and perspectives

Over the past decade, significant advancements in traditional non-contact sensors and tele-perception systems have laid

Reproduced from ref. 73 with permission from Wiley-VCH, copyright 2021. (g) A commercial vehicle speed sensor system. Reproduced from ref. 72 with permission from Elsevier, copyright 2023. (h) Non-contact limit alarm with multi-channel signal acquisition function. Reproduced from ref. 173 with permission from Wiley-VCH, copyright 2022. (i) A non-contact motion vector sensor. Reproduced from ref. 173 with permission from Wiley-VCH, copyright 2022. (j) Application of non-contact hand sanitizer. Reproduced from ref. 69 with permission from Wiley-VCH, copyright 2022. (k) Non-contact sensors for hydrological measurements and geological resource exploration. Reproduced from ref. 175 with permission from Elsevier, copyright 2024. (l) Non-contact monitoring of human motion trajectories. Reproduced from ref. 178 with permission from IEEE, copyright 2022. (m) Time domain and frequency domain analysis of walking for indoor navigation. Reproduced from ref. 71 with permission from Wiley-VCH, copyright 2022. (n) Blind navigation sensor based on triboelectrification and electrostatic induction. Reproduced from ref. 177 with permission from Elsevier, copyright 2022.

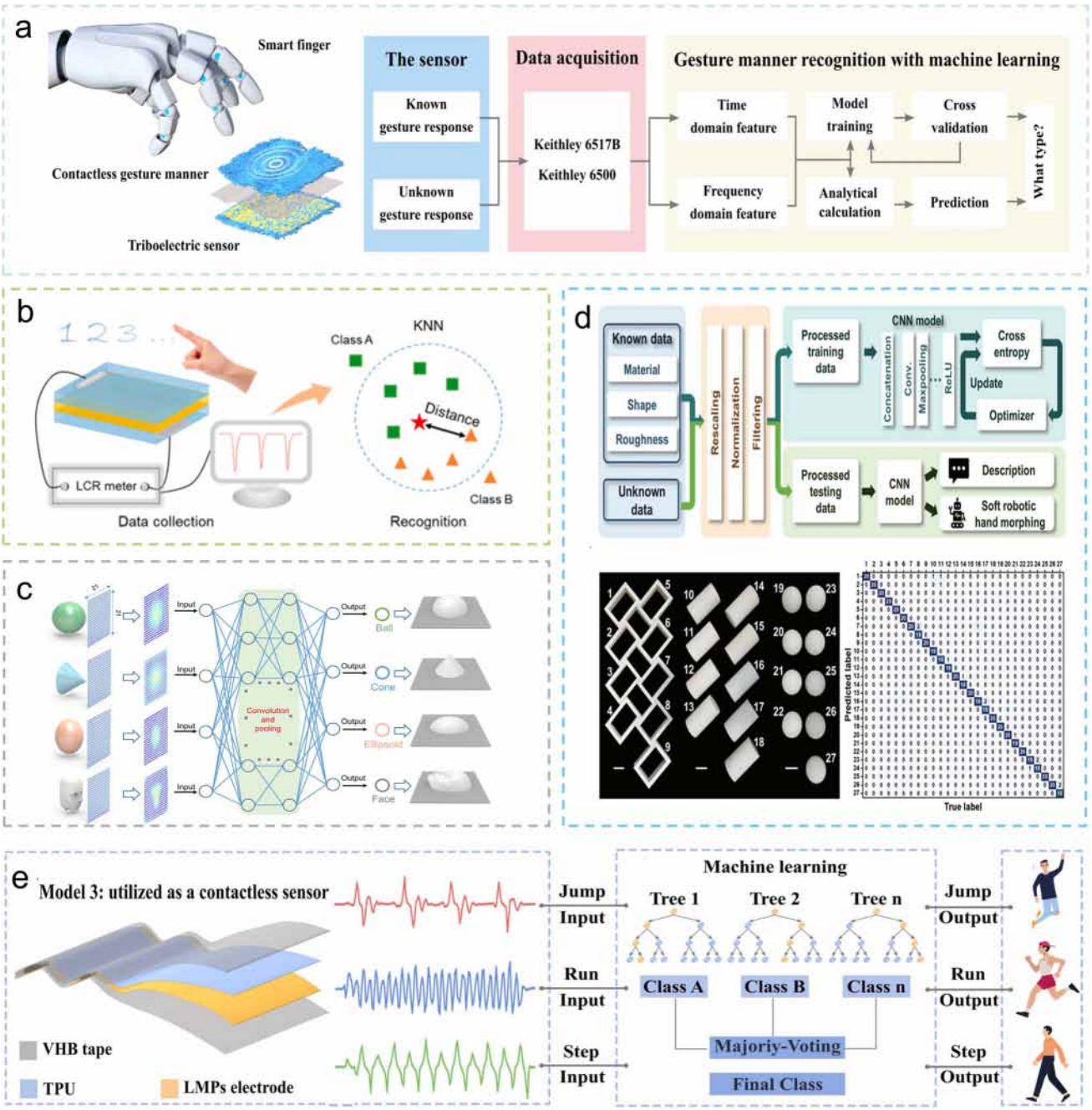

Fig. 15 Applications of traditional non-contact sensors in machine learning assistant system. (a) Real-time non-contact gesture recognition system utilized PCA. Reproduced from ref. 180 with permission from Donghua University, copyright 2024. (b) Proximity sensor in non-contact digital recognition based on the *K*NN. Reproduced from ref. 113 with permission from Elsevier, copyright 2022. (c) The 3D object recognition system based on the bioinspired electroreceptor matrix (21 × 21 units) and the CNN. Reproduced from ref. 70 with permission from the American Association for the Advancement of Science, copyright 2022. (d) An intelligent soft robot system integrated CNN that described the physical properties (material, shape and roughness) of objects in a linguistic way. Reproduced from ref. 181 with permission from Wiley-VCH, copyright 2023. (e) Non-contact sensors based on RF for motion pattern recognition. Reproduced from ref. 182 with permission from Elsevier, copyright 2023.

a solid foundation for enhancing embodied perception. This review provided a comprehensive review of the paradigm shift from traditional non-contact sensors to tele-perception, highlighting its potential for enabling innovative perception experiences by analyzing the current technological status. Traditional non-contact sensing technologies were categorized into electronic and ionic receptors, focusing on their operating principles, typical architectures, and performance optimization strategies. For electronic receptors, advancements included material composite design, chemical modification and structural optimization to improve charge capture ability. Ionic receptors addressed challenges such as liquid leakage and

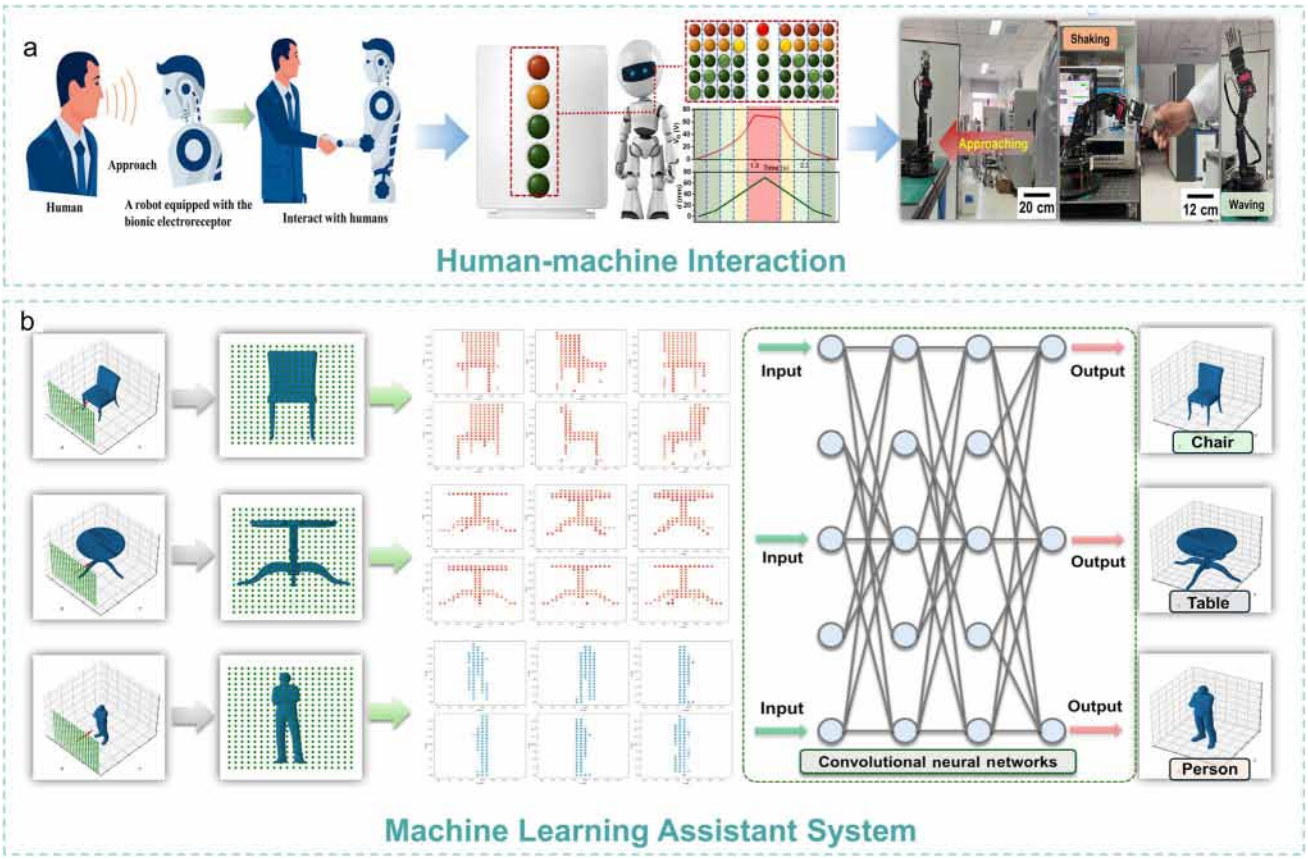

Fig. 16 Applications of tele-perception systems. (a) The application of bionic electroreceptor in HMI including virtual distance alarm robots and operating robot arms to wave and shake hands when adults are approaching. (b) The application of bionic electroreceptor in ML assistant system: the 3D object tele-perception system based on the bionic electroreceptor matrix (20 × 20 units) and the CNN. Reproduced from ref. 62 with permission from the American Association for the Advancement of Science, copyright 2024.

evaporation through conductive nanochannels and molecular synergy. Despite notable progress, challenges remain in sensitivity regulation and range expansion. This review examined the realization of tele-perception systems, with a focus on the critical role of charge-trapping strategies in enhancing charge stability. Key approaches include (i) promoting ion-selective migration and constructing deep charge traps, (ii) introducing interface layers to prolong charge retention, and (iii) doping with nanoparticles to enhance performance. Algorithmic advancements, such as multi-data fusion and neuromorphic sensing architecture designs, were also essential for improving system efficiency. Additionally, this article explored the wide applications of traditional non-contact sensing and tele-perception technologies in HMI, intelligent monitoring, and machine learning assistant systems, underscoring their potential for practical deployment. It highlights the role of electrostatic charge-trapping strategies in performance optimization and explores the integration of advanced sensing platforms with deep learning architectures, presenting a novel approach to advancing embodied intelligence. However, challenges persist in achieving efficient charge-trapping, particularly in maintaining effective electrostatic charge retention and ensuring algorithm adaptability in dynamic environments. These challenges necessitate further innovation in charge-trapping strategies and the development of collaborative optimization algorithms. Through a systematic examination of the core principles, structural designs, and performance optimization strategies, we offer valuable insights into the current state of research and highlight the transformative potential of tele-perception systems. We propose a roadmap that addresses multiple key areas to advance research and industrial development, as depicted in Fig. 17. First, continuous exploration of novel materials and electrostatic charge-trapping mechanisms is essential to enhance the sensitivity and detection range of tele-perception systems. Second, the development of advanced algorithms that enable multi-data fusion and adaptive learning is crucial for improving the accuracy and reliability of tele-perception. Finally, promoting the integration of tele-perception systems with existing HMIs and industrial automation platforms for advancing applications in pervasive sensing and embodied artificial intelligence.

5.1 Advancing charge-trapping strategies for enhanced tele-perception

An effective electrostatic charge-trapping strategy is pivotal for enhancing the accuracy and stability of tele-perception systems,

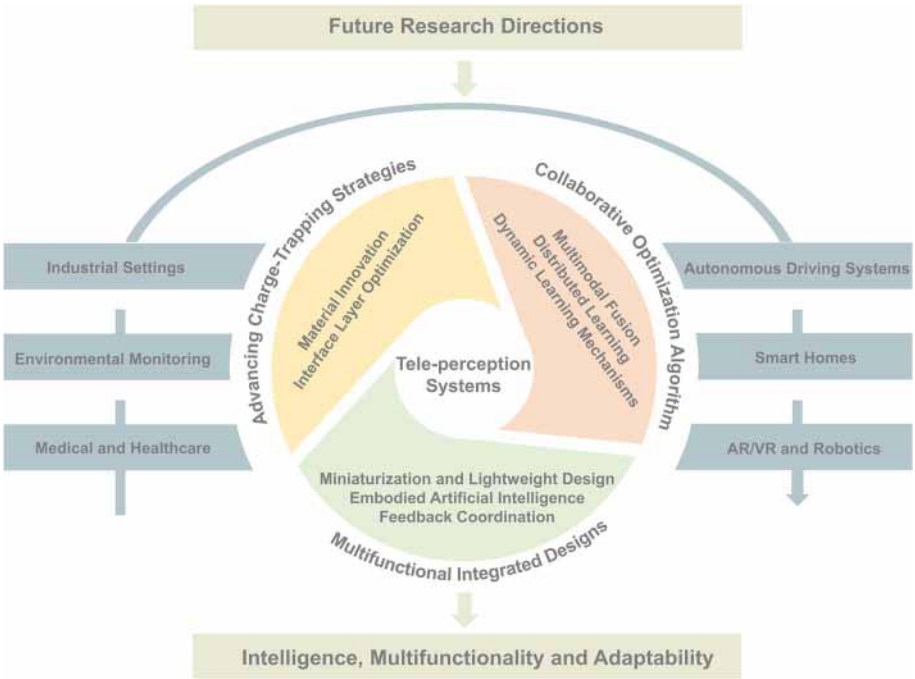

Fig. 17 The prospects in sustainable development of tele-perception systems.

especially in extending sensing range and enabling precise long-distance detection. However, persistent challenges, such as insufficient electrostatic charge trapping, limited retention capacity, and uneven electric field distribution, continue to hinder optimal performance. Especially environmental fluctuations, such as changes in temperature and humidity, can lead to charge leakage, undermining the stability of the charge-trapping mechanism. Despite advancements in optimizing charge-trapping structures, long-term retention remains a critical issue. Current approaches, such as multi-layer stacking to augment charge storage and transmission, often lead to increased structural complexity and diminished adaptability for advanced applications. To overcome these limitations, innovations in material design and interface layer optimization present promising solutions. Developing materials with high charge storage capacity, stability, flexibility, and self-healing properties is crucial for improving triboelectric performance while maintaining mechanical durability. Intelligent response materials that simulate the biological skin properties, combined with multifunctional bionic structures, could enable self-regulate based on changes in the external environment, thereby achieving more natural and comprehensive sensing capabilities. Advanced interface layer designs are equally essential. Simplified architectures that integrate charge blocking, storage, and transport functionalities can enhance efficiency. For example, gradient-functional interface layers, which dynamically adjust charge transport pathways and storage sites in response to varying electric fields, can improve charge retention and field uniformity. Dynamic adaptive layers, utilizing shape-memory or thermally and electrically responsive materials, further refine electric field distribution. Incorporating bionic microchannel networks into interface layers optimizes signal transmission, thus enhancing device efficiency and overall performance. Addressing these challenges through such advancements will significantly improve sensing accuracy, reliability, and scalability, paving the way for broader applications of tele-perception in intelligent systems and HMI.

5.2 Collaborative optimization algorithm for tele-perception

Integrating tele-perception system with intelligent algorithms is crucial for emulating the tactile perception of human skin, thereby enabling more refined interactions and enhanced environmental awareness. Current challenges lie on environmental robustness, especially multimodal interaction (recognizing complex behavioral patterns, distinguishing various object types and adapting accurately to dynamic environmental changes). Moreover, deviations in the training data may result in biased or unfair model output results. These limitations arise from the inherent complexity of real-world scenarios, where traditional sensing mechanisms struggle with low signal-to-noise ratios, limited adaptability, and difficulties in processing large volumes of unstructured data in real time. The robustness of the algorithms deployed in real-world applications must be capable of adapting to environmental variability, such as sensor noise and external disturbances, to maintain consistent performance. While techniques like adaptive pulse recognition can enhance adaptability, achieving reliable precision under fluctuating conditions remains a challenge. Collaborative optimization of intelligent algorithms addresses these issues through multimodal fusion, federated learning, distributed learning, and dynamic learning mechanisms. At the same time, the integration of quantum computing is expected

to significantly enhance data-processing speed, particularly when handling high-dimensional data. A unified multimodal representation framework, powered by DL algorithms, enables seamless cross-modal collaboration, while feature compensation techniques enhance data integration by exploiting the strengths of diverse sensing modalities. Dynamic learning mechanisms, utilizing the spatial and temporal characteristics of distributed data, improve algorithm adaptability across varied scenarios. For complex pattern recognition, CNNs excel at processing spatial data for gesture recognition and object classification, while RNNs are particularly effective for tracking dynamic behaviors and monitoring environmental changes. ML models such as SVMs and adaptive boosting (AdaBoost) refine detection thresholds and minimize noise in sensitive applications. Reinforcement learning further optimizes sensing parameters in real time, enhancing responsiveness and accuracy in dynamic environments. These customized algorithms significantly enhance the perceptual capabilities of tele-perception systems, enabling intelligent interaction and decision making in complex settings. Moreover, future research will focus on developing interpretable artificial intelligence to enhance the transparency of decision-making processes in tele-perception applications. And the incorporation of feedback mechanisms allows the system to predict and adapt to user behavior, improving efficiency in human-machine collaboration and decision support.

5.3 Multifunctional integration and applications in tele-perception

The multifunctional integration of tele-perception systems is essential for advancing applications in pervasive sensing and embodied artificial intelligence. However, the integration with existing technologies such as HMI and industrial automation platforms presents a significant challenge. Future developments will prioritize miniaturization, integration, wearability, and self-powering, leveraging micro–nano processing and edge computing to incorporate sensors, processing chips, and communication modules into compact systems. These systems will enable localized data processing, reducing reliance on cloud computing and enhancing overall efficiency. In addition, the expansion of additive manufacturing technology and cloud collaborative manufacturing will facilitate the wider application of tele-perception systems. Tele-perception technology is transforming a wide array of fields. In industrial settings, it facilitates real-time monitoring and dynamic optimization of production processes, thereby improving flexibility and minimizing errors. Environmental monitoring benefits from precise detection of subtle changes, such as gas leaks or vibrations, providing early warnings for disasters and industrial accidents. In medical and healthcare, tele-perception enables real-time health monitoring, elderly care, and precision surgery, fostering proactive and personalized medicine. Autonomous driving systems utilize tele-perception for improved environmental awareness and safe navigation in complex scenarios. In smart homes, it enables dynamic adjustments to user preferences, while AR and VR applications benefit from the seamless integration of real and virtual environments, enhancing immersion and interactivity. In robotics, tele-perception enhances adaptability and autonomous decision making, driving innovation across industrial, medical, and service sectors. This integration highlights the transformative potential of tele-perception in revolutionizing intelligent systems and expanding their practical applications.

Data availability

Data availability is not applicable to this article as no new data were created or analyzed in this study.

Author contributions

J. X. G. and Y. D. were responsible for writing the original draft, while J. X. G., Y. D., and D. W. contributed to the review and editing. J. X. G., Y. D., and D. W. provided supervision, and D. W. and Z. L. W. handled project administration. All authors have read and approved the final version of the manuscript.

Conflicts of interest

The authors declare no conflict of interest.

Acknowledgements

This work was supported by the National Natural Science Foundation (Grant No. 22479016).

References

1 C. Bartolozzi, G. Indiveri and E. Donati, *Nat. Commun.*, 2022, **13**, 1024.
2 R. Chrisley, *Artif. Intell.*, 2003, **149**, 131–150.
3 D. Jin and L. Zhang, *Nat. Mach. Intell.*, 2020, **2**, 663–664.
4 X. Shi, J. Luo, J. Luo, X. Li, K. Han, D. Li, X. Cao and Z. Wang, *ACS Nano*, 2022, **16**, 3341–3350.
5 C. M. Boutry, M. Negre, M. Jorda, O. Vardoulis, A. Chortos, O. Khatib and Z. Bao, *Sci. Robot.*, 2018, **3**, eaau6914.
6 Y. Yan, Z. Hu, Z. Yang, W. Yuan, C. Song, J. Pan and Y. Shen, *Sci. Robot.*, 2021, **6**, eabc8801.
7 Y.-C. Lai, R. Liu, M. Xu and C. Zhao, *Handbook of Triboelectric Nanogenerators*, 2023, pp. 1–52.
8 H. Kong, W. Li, Z. Song and L. Niu, *Mater. Futures*, 2024, **3**, 022501.
9 Y. Gao, K. Yao, S. Jia, Y. Huang, G. Zhao, B. Zhang, Y. Liu and X. Yu, *Matter*, 2024, **7**, 2826–2845.
10 C. Chiu, S. Chen, Y. Pao, M. Huang, S. Chan and Z. Lin, *Sci. Technol. Adv. Mater.*, 2019, **20**, 964–971.
11 G. Qu, X. Li, L. Hu and G. Jiang, *Environ. Sci. Technol.*, 2020, **54**, 3730–3732.
12 H. S. Kang, S. W. Han, C. Park, S. W. Lee, H. Eoh, J. Baek, D.-G. Shin, T. H. Park, J. Huh, H. Lee, D.-E. Kim, D. Y. Ryu, E. L. Thomas, W.-G. Koh and C. Park, *Sci. Adv.*, 2020, **6**, eabb5769.

13 L. Mennel, J. Symonowicz, S. Wachter, D. K. Polyushkin, A. J. Molina-Mendoza and T. Mueller, *Nature*, 2020, **579**, 62–66.
14 F. Zhou, Z. Zhou, J. Chen, T. H. Choy, J. Wang, N. Zhang, Z. Lin, S. Yu, J. Kang, H. S. P. Wong and Y. Chai, *Nat. Nanotechnol.*, 2019, **14**, 776–782.
15 O. K. Oyedotun and A. Khashman, *Neural Comput. Appl.*, 2017, **28**, 3941–3951.
16 S. D. Min, J. K. Kim, H. S. Shin, Y. H. Yun, C. K. Lee and M. Lee, *IEEE Sens. J.*, 2010, **10**, 1732–1739.
17 A. Sun, Z. Wu, D. Fang, J. Zhang and W. Wang, *IEEE Sens. J.*, 2016, **16**, 5632–5635.
18 S. Kim and H. Kim, *Int. J. Control Autom. Syst.*, 2010, **8**, 1280–1287.
19 N. Jeger-Madiot, J. Gateau, M. Fink and R.-K. Ing, *Med. Eng. Phys.*, 2017, **50**, 96–102.
20 Y. S. Suh, *Sensors*, 2019, **19**, 1924.
21 X. Lin, Y. Liang, L. Jin and L. Wang, *Sensors*, 2019, **19**, 4632.
22 X. Zhou, Z. Li, C. Ge, B. Fan. and P. Wang, *Opt. Quantum Electron.*, 2018, **51**, 14.
23 D. Um, D. Ryu and M. Kal, *IEEE Sens. J.*, 2011, **11**, 3352–3358.
24 K. Kito, S. Kitajima, T. Matsuda, M. Inoue, M. Tamura and M. Kimura, *J. Soc. Inf. Disp.*, 2019, **27**, 147–154.
25 D. Popa and F. Udrea, *Sensors*, 2019, **19**, 2076.
26 S. An, H. Zhu, C. Guo, B. Fu, C. Song, P. Tao, W. Shang and T. Deng, *Nat. Commun.*, 2022, **13**, 1446.
27 K. Liu, W. Wang, Y. Yu, X. Hou, Y. Liu, W. Chen, X. Wang, J. Lu and Z. Ni, *Nano Lett.*, 2019, **19**, 8132–8137.
28 P. Makushko, E. S. Oliveros Mata, G. S. Cañón Bermúdez, M. Hassan, S. Laureti, C. Rinaldi, F. Fagiani, G. Barucca, N. Schmidt, Y. Zabila, T. Kosub, R. Illing, O. Volkov, I. Vladymyrskyi, J. Fassbender, M. Albrecht, G. Varvaro and D. Makarov, *Adv. Funct. Mater.*, 2021, **31**, 2170184.
29 M. Ha, G. S. Cañón Bermúdez, T. Kosub, I. Mönch, Y. Zabila, E. S. Oliveros Mata, R. Illing, Y. Wang, J. Fassbender and D. Makarov, *Adv. Mater.*, 2021, **33**, 2005521.
30 B. Zhang, Z. Xiang, S. Zhu, Q. Hu, Y. Cao, J. Zhong, Q. Zhong, B. Wang, Y. Fang, B. Hu, J. Zhou and Z. Wang, *Nano Res.*, 2014, **7**, 1488–1496.
31 M. S. Sarwar, Y. Dobashi, C. Preston, J. K. M. Wyss, S. Mirabbasi and J. D. W. Madden, *Sci. Adv.*, 2017, **3**, e1602200.
32 J. Ge, X. Wang, M. Drack, O. Volkov, M. Liang, G. S. Cañón Bermúdez, R. Illing, C. Wang, S. Zhou, J. Fassbender, M. Kaltenbrunner and D. Makarov, *Nat. Commun.*, 2019, **10**, 4405.
33 F. Guan, Y. Xie, H. Wu, Y. Meng, Y. Shi, M. Gao, Z. Zhang, S. Chen, Y. Chen, H. Wang and Q. Pei, *ACS Nano*, 2020, **14**, 15428–15439.
34 L. Lu, C. Jiang, G. Hu, J. Liu and B. Yang, *Adv. Mater.*, 2021, **33**, 2100218.
35 T. Yamada, Y. Hayamizu, Y. Yamamoto, Y. Yomogida, A. Izadi-Najafabadi, D. N. Futaba and K. Hata, *Nat. Nanotechnol.*, 2011, **6**, 296–301.
36 W. Liu, M.-S. Song, B. Kong and Y. Cui, *Adv. Mater.*, 2017, **29**, 1603436.
37 S.-B. Jeon, Y.-H. Nho, S.-J. Park, W.-G. Kim, I.-W. Tcho, D. Kim, D.-S. Kwon and Y.-K. Choi, *Nano Energy*, 2017, **41**, 139–147.
38 D. J. Schlegel, D. P. Finkbeiner and M. Davis, *Astrophys. J.*, 1998, **500**, 525.
39 D. Rodrigues-Bigaton, A. V. Dibai Filho, A. C. d. S. Costa, A. C. Packer and E. M. de Castro, *J. Manip. Physiol. Ther.*, 2013, **36**, 253–258.
40 H. Yang, M. Deng, Q. Tang, W. He, C. Hu, Y. Xi, R. Liu and Z. Wang, *Adv. Energy Mater.*, 2019, **9**, 1901149.
41 Z. Wang, J. Chen and L. Lin, *Energy Environ. Sci.*, 2015, **8**, 2250–2282.
42 Z. Wang, *Adv. Mater.*, 2012, **24**, 280–285.
43 Z. Wang, G. Zhu, Y. Yang, S. Wang and C. Pan, *Mater. Today*, 2012, **15**, 532–543.
44 F. Yi, L. Lin, S. Niu, J. Yang, W. Wu, S. Wang, Q. Liao, Y. Zhang and Z. Wang, *Adv. Funct. Mater.*, 2014, **24**, 7488–7494.
45 F. Fan, Z. Tian and Z. Wang, *Nano Energy*, 2012, **1**, 328–334.
46 X. Pu, H. Guo, Q. Tang, J. Chen, L. Feng, G. Liu, X. Wang, Y. Xi, C. Hu and Z. Wang, *Nano Energy*, 2018, **54**, 453–460.
47 F. Wen, Z. Sun, T. He, Q. Shi, M. Zhu, Z. Zhang, L. Li, T. Zhang and C. Lee, *Advanced Science*, 2020, **7**, 2000261.
48 M. Wang, Z. Yan, T. Wang, P. Cai, S. Gao, Y. Zeng, C. Wan, H. Wang, L. Pan, J. Yu, S. Pan, K. He, J. Lu and X. Chen, *Nat. Electron.*, 2020, **3**, 563–570.
49 H. Wu, Z. Su, M. Shi, L. Miao, Y. Song, H. Chen, M. Han and H. Zhang, *Adv. Funct. Mater.*, 2018, **28**, 1704641.
50 Y. Tang, H. Zhou, X. Sun, N. Diao, J. Wang, B. Zhang, C. Qin, E. Liang and Y. Mao, *Adv. Funct. Mater.*, 2020, **30**, 1907893.
51 Y. Du, P. Shen, H. Liu, Z. Zhang, T. Ren, R. Shi, Z. Wang and D. Wei, *Adv. Funct. Mater.*, 2024, **34**, 2409602.
52 P. K. Sarkar, T. Kamilya and S. Acharya, *ACS Appl. Energy Mater.*, 2019, **2**, 5507–5514.
53 Y. Jiang, K. Dong, J. An, F. Liang, J. Yi, X. Peng, C. Ning, C. Ye and Z. Wang, *ACS Appl. Mater. Interfaces*, 2021, **13**, 11205–11214.
54 Z. Lin, Z. Wu, B. Zhang, Y.-C. Wang, H. Guo, G. Liu, C. Chen, Y. Chen, J. Yang and Z. Wang, *Adv. Mater. Technol.*, 2019, **4**, 1800360.
55 X. Li, S. Li, X. Guo, J. Shao, Z. Wang and D. Wei, *Matter*, 2023, **6**, 3912–3926.
56 Y. Du, S. Fu, C. Shan, H. Wu, W. He, J. Wang, H. Guo, G. Li, Z. Wang and C. Hu, *Adv. Funct. Mater.*, 2022, **32**, 2208783.
57 W. He, C. Shan, H. Wu, S. Fu, Q. Li, G. Li, X. Zhang, Y. Du, J. Wang, X. Wang and C. Hu, *Adv. Energy Mater.*, 2022, **12**, 2201454.
58 W. He, C. Shan, S. Fu, H. Wu, J. Wang, Q. Mu, G. Li and C. Hu, *Adv. Mater.*, 2023, **35**, 2209657.
59 M. Salauddin, S. M. S. Rana, M. Sharifuzzaman, S. H. Lee, M. A. Zahed, Y. Do Shin, S. Seonu, H. S. Song, T. Bhatta and J. Y. Park, *Nano Energy*, 2022, **100**, 107462.
60 C. Zhao, Z. Wang, Y. Wang, Z. Qian, Z. Tan, Q. Chen, X. Pan, M. Xu and Y.-C. Lai, *Adv. Funct. Mater.*, 2023, **33**, 2306381.
61 Y. Xi, J. Hua and Y. Shi, *Nano Energy*, 2020, **69**, 104390.

62 Y. Du, P. Shen, H. Liu, Y. Zhang, L. Jia, X. Pu, F. Yang, T. Ren, D. Chu, Z. Wang and D. Wei, *Sci. Adv.*, 2024, **10**, eadp8681.
63 Y. Du, Z. Wang and D. Wei, *Sci. Bull.*, 2025, DOI: **10.1016/j.scib.2025.02.014**.
64 T. Feng, D. Ling, C. Li, W. Zheng, S. Zhang, C. Li, A. Emel'yanov, A. S. Pozdnyakov, L. Lu and Y. Mao, *Nano Res.*, 2024, **17**, 4462–4470.
65 B. Wang, M. Gao, X. Fu, M. Geng, Y. Liu, N. Cheng, J. Li, L. Li, Z. Zhang and Y. Song, *Nano Energy*, 2023, **107**, 108135.
66 N. Dai, X. Guan, C. Lu, K. Zhang, S. Xu, I. M. Lei, G. Li, Q. Zhong, P. Fang and J. Zhong, *ACS Nano*, 2023, **17**, 24814–24825.
67 Z. Hou, T. Liu, M. Li, Y. Xu, X. Wu, S. Luo, C. Cai, Y. Mou, Y. Qiu, S. Nie and D. Lu, *Adv. Funct. Mater.*, 2024, **34**, 2400750.
68 H. Guo, X. Jia, L. Liu, X. Cao, N. Wang and Z. Wang, *ACS Nano*, 2018, **12**, 3461–3467.
69 K. Shrestha, S. Sharma, G. B. Pradhan, T. Bhatta, P. Maharjan, S. M. S. Rana, S. Lee, S. Seonu, Y. Shin and J. Y. Park, *Adv. Funct. Mater.*, 2022, **32**, 2113005.
70 Z. Guo, H. Wang, J. Shao, Y. Shao, L. Jia, L. Li, X. Pu and Z. Wang, *Sci. Adv.*, 2022, **8**, eabo5201.
71 W. Zhang, Y. Lu, T. Liu, J. Zhao, Y. Liu, Q. Fu, J. Mo, C. Cai and S. Nie, *Small*, 2022, **18**, 2200577.
72 G. H. Han, S. H. Lee, J. Gao, H. S. Shin, J. W. Lee, K. J. Choi, Y. Yang, H.-C. Song, Y. Kim and J. M. Baik, *Nano Energy*, 2023, **112**, 108428.
73 S. M. S. Rana, M. A. Zahed, M. T. Rahman, M. Salauddin, S. H. Lee, C. Park, P. Maharjan, T. Bhatta, K. Shrestha and J. Y. Park, *Adv. Funct. Mater.*, 2021, **31**, 2105110.
74 J. W. Lee, S. Jung, J. Jo, G. H. Han, D.-M. Lee, J. Oh, H. J. Hwang, D. Choi, S.-W. Kim, J. H. Lee, C. Yang and J. M. Baik, *Energy Environ. Sci.*, 2021, **14**, 1004–1015.
75 J. Ma, J. Zhu, P. Ma, Y. Jie, Z. Wang and X. Cao, *ACS Energy Lett.*, 2020, **5**, 3005–3011.
76 S. Chen, Y. Wang, L. Yang, Y. Guo, M. Wang and K. Sun, *Nano Energy*, 2021, **82**, 105719.
77 F. Wang, Z. Ren, J. Nie, J. Tian, Y. Ding and X. Chen, *Adv. Mater. Technol.*, 2020, **5**, 1900789.
78 S. Chou, Y. Chen, Z. Yan, T. Lu, T. Wu, M. Lu, T. Ko, W. Peng, J. Chen, F. Hsu, S. Chen, C. Chen and Y. Lai, *Adv. Energy Mater.*, 2024, **14**, 2470156.
79 T. Ficker, *J. Electrost.*, 2006, **64**, 10–16.
80 K. Takiguchi, T. Wada and S. Toyama, *J. Adv. Mech. Des. Syst. Manuf.*, 2007, **1**, 294–305.
81 C. Yang and Z. Suo, *Nat. Rev. Mater.*, 2018, **3**, 125–142.
82 H. Chun and T. D. Chung, *Annu. Rev. Anal. Chem.*, 2015, **8**, 441–462.
83 Y. Hou and X. Hou, *Science*, 2021, **373**, 628–629.
84 J.-Y. Sun, C. Keplinger, G. M. Whitesides and Z. Suo, *Adv. Mater.*, 2014, **26**, 7608–7614.
85 Y. Wu, Y. Luo, T. J. Cuthbert, A. V. Shokurov, P. K. Chu, S.-P. Feng and C. Menon, *Adv. Sci.*, 2022, **9**, 2106008.
86 J. Zhou, H. Wang, C. Du, D. Zhang, H. Lin, Y. Chen and J. Xiong, *Adv. Energy Sustainability Res.*, 2022, **3**, 2100161.
87 S. Niu, Y. Liu, S. Wang, L. Lin, Y. S. Zhou, Y. Hu and Z. Wang, *Adv. Funct. Mater.*, 2014, **24**, 3332–3340.
88 B. Chen, Y. Yang and Z. Wang, *Adv. Energy Mater.*, 2018, **8**, 1702649.
89 W. Song, X. Wang, H. Qiu, Q. Liu, J. Zhang, Z. Fan, M. Yu, S. Ramakrishna, H. Hu and Y. Long, *Nano Energy*, 2019, **63**, 103878.
90 Y. S. Choi, S.-W. Kim and S. Kar-Narayan, *Adv. Energy Mater.*, 2021, **11**, 2003802.
91 M. Salauddin, S. M. S. Rana, M. Sharifuzzaman, M. T. Rahman, C. Park, H. Cho, P. Maharjan, T. Bhatta and J. Y. Park, *Adv. Energy Mater.*, 2021, **11**, 2002832.
92 T. Bhatta, P. Maharjan, H. Cho, C. Park, S. H. Yoon, S. Sharma, M. Salauddin, M. T. Rahman, S. M. S. Rana and J. Y. Park, *Nano Energy*, 2021, **81**, 105670.
93 M. Salauddin, S. M. S. Rana, M. T. Rahman, M. Sharifuzzaman, P. Maharjan, T. Bhatta, H. Cho, S. H. Lee, C. Park, K. Shrestha, S. Sharma and J. Y. Park, *Adv. Funct. Mater.*, 2022, **32**, 2107143.
94 X. Luo, L. Zhu, Y. Wang, J. Li, J. Nie and Z. Wang, *Adv. Funct. Mater.*, 2021, **31**, 2104928.
95 C. Jiang, C. Wu, X. Li, Y. Yao, L. Lan, F. Zhao, Z. Ye, Y. Ying and J. Ping, *Nano Energy*, 2019, **59**, 268–276.
96 C. Jiang, X. Li, Y. Yao, L. Lan, Y. Shao, F. Zhao, Y. Ying and J. Ping, *Nano Energy*, 2019, **66**, 104121.
97 H. Zou, Y. Zhang, L. Guo, P. Wang, X. He, G. Dai, H. Zheng, C. Chen, A. Wang, C. Xu and Z. Wang, *Nat. Commun.*, 2019, **10**, 1427.
98 M. Seol, S. Kim, Y. Cho, K.-E. Byun, H. Kim, J. Kim, S. K. Kim, S.-W. Kim, H.-J. Shin and S. Park, *Adv. Mater.*, 2018, **30**, 1801210.
99 Z. Wang, *ACS Nano*, 2013, **7**, 9533–9557.
100 F. Fan, L. Lin, G. Zhu, W. Wu, R. Zhang and Z. Wang, *Nano Lett.*, 2012, **12**, 3109–3114.
101 K. Y. Lee, H. J. Yoon, T. Jiang, X. Wen, W. Seung, S. Kim and Z. Wang, *Adv. Energy Mater.*, 2016, **6**, 1502566.
102 Q. Ling, W. Liu, J. Liu, L. Zhao, Z. Ren and H. Gu, *ACS Appl. Mater. Interfaces*, 2022, **14**, 24741–24754.
103 L. Chen, X. Fei, Y. Zhou, J. Tian, L. Xu and Y. Li, *J. Colloid Interface Sci.*, 2022, **628**, 287–298.
104 L. Xia, R. Xie, X. Ju, W. Wang, Q. Chen and L. Chu, *Nat. Commun.*, 2013, **4**, 2226.
105 R. Liu, K. Chen, H. Liu, Y. Liu, R. Cong, J. Guo and Y. Tian, *ACS Appl. Mater. Interfaces*, 2022, **14**, 51341–51350.
106 J. P. Gong, Y. Katsuyama, T. Kurokawa and Y. Osada, *Adv. Mater.*, 2003, **15**, 1155–1158.
107 F. Huang, W. Wei, Q. Fan, L. Li, M. Zhao and Z. Zhou, *J. Colloid Interface Sci.*, 2022, **615**, 215–226.
108 C. Keplinger, J.-Y. Sun, C. C. Foo, P. Rothemund, G. M. Whitesides and Z. Suo, *Science*, 2013, **341**, 984–987.
109 K. Qian, J. Zhou, M. Miao, S. Thaiboonrod, J. Fang and X. Feng, *Composites, Part B*, 2024, **287**, 111826.
110 Y. Ma, K. Liu, L. Lao, X. Li, Z. Zhang, S. Lu, Y. Li and Z. Li, *Int. J. Biol. Macromol.*, 2022, **205**, 491–499.
111 K. Parida, G. Thangavel, G. Cai, X. Zhou, S. Park, J. Xiong and P. S. Lee, *Nat. Commun.*, 2019, **10**, 2158.

112 R. Ji, S. Yan, Z. Zhu, Y. Wang, D. He, K. Wang, D. Zhou, Q. Jia, X. Wang, B. Zhang, C. Shi, T. Xu, R. Wang, R. Wang and Y. Zhou, *Adv. Sci.*, 2024, **11**, 2401869.
113 Y. Chen, C. Zhang, R. Yin, A. Yin, Q. Feng, F. Liu, J. Shao, T. Su, H. Wang, G. Chen and W. Zhao, *Chem. Eng. J.*, 2022, **449**, 137907.
114 F. Yang, P. Peng, Z.-Y. Yan, H. Fan, X. Li, S. Li, H. Liu, T. Ren, Y. Zhou, Z. Wang and D. Wei, *Nat. Energy*, 2024, **9**, 263–271.
115 X. Li, R. Li, S. Li, Z. Wang and D. Wei, *Nat. Commun.*, 2024, **15**, 6182.
116 Y. Ouyang, X. Li, S. Li, P. Peng, F. Yang, Z. Wang and D. Wei, *Nano Energy*, 2023, **116**, 108796.
117 W. Xu, Y. Nan, Y. Jin, X. Chen, M. Xie, C. Chen and C. Zhao, *Chem. Mater.*, 2022, **34**, 8740–8748.
118 H. Peng, Y. Xin, J. Xu, H. Liu and J. Zhang, *Mater. Horiz.*, 2019, **6**, 618–625.
119 B. Chen, J. J. Lu, C. H. Yang, J. H. Yang, J. Zhou, Y. M. Chen and Z. Suo, *ACS Appl. Mater. Interfaces*, 2014, **6**, 7840–7845.
120 J. Wang, N. Zhang, Y. Tan, F. Fu, G. Liu, Y. Fang, X. Zhang, M. Liu, Y. Cheng and J. Yu, *ACS Appl. Mater. Interfaces*, 2022, **14**, 21945–21953.
121 M. Wang, H. Zhou, H. Du, L. Chen, G. Zhao, H. Liu, X. Jin, W. Chen and A. Ma, *Chem. Eng. J.*, 2022, **446**, 137163.
122 J. Zhou, F. Zhuo, X. Long, Y. Liu, H. Lu, J. Luo, L. Chen, S. Dong, Y. Fu and H. Duan, *Chem. Eng. J.*, 2022, **447**, 137259.
123 Z. Lei and P. Wu, *Nat. Commun.*, 2019, **10**, 3429.
124 P. Zhang, W. Guo, Z. Guo, Y. Ma, L. Gao, Z. Cong, X. Zhao, L. Qiao, X. Pu and Z. Wang, *Adv. Mater.*, 2021, **33**, 2101396.
125 B. Yiming, Y. Han, Z. Han, X. Zhang, Y. Li, W. Lian, M. Zhang, J. Yin, T. Sun, Z. Wu, T. Li, J. Fu, Z. Jia and S. Qu, *Adv. Mater.*, 2021, **33**, 2006111.
126 Y. Lee, S. H. Cha, Y.-W. Kim, D. Choi and J.-Y. Sun, *Nat. Commun.*, 2018, **9**, 1804.
127 H. Yuk, T. Zhang, G. A. Parada, X. Liu and X. Zhao, *Nat. Commun.*, 2016, **7**, 12028.
128 H. Yang, C. Li, M. Yang, Y. Pan, Q. Yin, J. Tang, H. Qi and Z. Suo, *Adv. Funct. Mater.*, 2019, **29**, 1901721.
129 C. Zhang, L. Zhou, P. Cheng, X. Yin, D. Liu, X. Li, H. Guo, Z. Wang and J. Wang, *Appl. Mater. Today*, 2020, **18**, 100496.
130 P. Yang, Y. Shi, X. Tao, Z. Liu, X. Dong, Z. Wang and X. Chen, *Matter*, 2023, **6**, 1295–1311.
131 X. Tao, P. Yang, Z. Liu, S. Qin, J. Hu, Z. Huang, X. Chen and J. Qu, *ACS Nano*, 2024, **18**, 4467–4477.
132 N. Wang, D. Yang, W. Zhang, M. Feng, Z. Li, E. Ye, X. J. Loh and D. Wang, *ACS Appl. Mater. Interfaces*, 2023, **15**, 997–1009.
133 Z. Liu, Y. Huang, Y. Shi, X. Tao, P. Yang, X. Dong, J. Hu, Z. Huang, X. Chen and J. Qu, *Adv. Funct. Mater.*, 2023, **33**, 2302164.
134 N. Wang, Y. Liu, Y. Feng, J. Yang, Y. Wu, B. Zhang, Y. Li, B. Li, S. Wang, E. Ye, Y.-W. Zhang, X. Loh, F. Zhou, Z. Li and D. Wang, *Adv. Mater.*, 2024, **36**, 2303389.
135 Y. Wang, Y. Li, S. Liu, F. Li, C. Zhu, S. Li and Y. Cheng, *Macromolecules*, 2016, **49**, 5444–5451.
136 N. Tang, J. Zhou, L. Wang, M. Stolte, G. Xie, X. Wen, L. Liu, F. Würthner, J. Gierschner and Z. Xie, *Nat. Commun.*, 2023, **14**, 1922.
137 S. Zhou, X. Tao, Z. Liu, H. Wu, Z. Guan, L. Liu, J. Li, X. Chen and W. Ou-Yang, *Adv. Funct. Mater.*, 2024, **34**, 2405443.
138 Z. Liu, Y. Huang, Y. Shi, X. Tao, H. He, F. Chen, Z. Huang, Z. Wang, X. Chen and J. Qu, *Nat. Commun.*, 2022, **13**, 4083.
139 N. Cui, L. Gu, Y. Lei, J. Liu, Y. Qin, X. Ma, Y. Hao and Z. Wang, *ACS Nano*, 2016, **10**, 6131–6138.
140 Y. Feng, Y. Zheng, G. Zhang, D. Wang, F. Zhou and W. Liu, *Nano Energy*, 2017, **38**, 467–476.
141 X. Xie, X. Chen, C. Zhao, Y. Liu, X. Sun, C. Zhao and Z. Wen, *Nano Energy*, 2021, **79**, 105439.
142 X. Xie, Y. Fang, C. Lu, Y. Tao, L. Yin, Y. Zhang, Z. Wang, S. Wang, J. Zhao, X. Tu, X. Sun, E. G. Lim, C. Zhao, Y. Liu and Z. Wen, *Chem. Eng. J.*, 2023, **452**, 139469.
143 L. Xie, L. Yin, Y. Liu, H. Liu, B. Lu, C. Zhao, T. A. Khattab, Z. Wen and X. Sun, *ACS Nano*, 2022, **16**, 5292–5302.
144 J. Du, J. Duan, X. Yang, Y. Wang, Y. Duan and Q. Tang, *Nano Energy*, 2020, **74**, 104845.
145 J. Wang, B. Zhang, Z. Zhao, Y. Gao, D. Liu, X. Liu, P. Yang, Z. Guo, Z. Wang and J. Wang, *Adv. Energy Mater.*, 2024, **14**, 2303874.
146 S. Sriphan, T. Charoonsuk, T. Maluangnont and N. Vittayakorn, *ACS Appl. Energy Mater.*, 2019, **2**, 3840–3850.
147 L. Li and M. Wu, *ACS Nano*, 2017, **11**, 6382–6388.
148 X. Suo, B. Li, H. Ji, S. Mei, S. Miao, M. Gu, Y. Yang, D. Jiang, S. Cui, L. Chen, G. Chen, Z. Wen and H. Huang, *Nano Energy*, 2023, **114**, 108651.
149 J. Duan, G. Yue, H. Li, T. Liu, P. Wang, W. Yu, P. Shang, C. Meng and S. Guo, *Nano Energy*, 2024, **128**, 109860.
150 Z. Li, J. Liu, M. Chi, X. Miao, H. Yang, W. Cui, A. Yu and J. Zhai, *Chem. Eng. J.*, 2024, **481**, 148726.
151 W. Li, Y. Xiang, W. Zhang, K. Loos and Y. Pei, *Nano Energy*, 2023, **113**, 108539.
152 A. Mondal, M. Faraz, M. Dahiya and N. Khare, *ACS Appl. Mater. Interfaces*, 2024, **16**, 50659–50670.
153 Q. Li, O. Kroemer, Z. Su, F. F. Veiga, M. Kaboli and H. J. Ritter, *IEEE Trans. Robot.*, 2020, **36**, 1619–1634.
154 R. Li, D. Wei and Z. Wang, *Nanomaterials*, 2024, **14**, 165.
155 V. D. Sánchez A, *Neurocomputing*, 2003, **55**, 5–20.
156 J. L. Speiser, M. E. Miller, J. Tooze and E. Ip, *Expert Syst. Appl.*, 2019, **134**, 93–101.
157 J. A. Romero-del-Castillo, M. Mendoza-Hurtado, D. Ortiz-Boyer and N. García-Pedrajas, *Eng. Appl. Artif. Intell.*, 2022, **116**, 105487.
158 H. Zhang, L. Feng, X. Zhang, Y. Yang and J. Li, *Digit. Signal Process.*, 2022, **123**, 103397.
159 W. De Mulder, S. Bethard and M.-F. Moens, *Comput. Speech Lang.*, 2015, **30**, 61–98.
160 Y. Wu and J. Feng, *Wirel. Pers. Commun.*, 2018, **102**, 1645–1656.
161 J. Lever, M. Krzywinski and N. Altman, *Nat. Methods*, 2017, **14**, 641–642.
162 J. R. Quinlan, *Machine Learning*, 1986, **1**, 81–106.
163 I. O. Tolstikhin, N. Houlsby, A. Kolesnikov, L. Beyer, X. Zhai, T. Unterthiner, J. Yung, D. Keysers, J. Uszkoreit,

M. Lucic and A. Dosovitskiy, *Adv. Neural Inf. Process Syst.*, 2021, **34**, 24261–24272.
164 T. Chen and C. Guestrin, presented in part at the *Proceedings of the 22nd ACM SIGKDD International Conference on Knowledge Discovery and Data Mining*, San Francisco, California, USA, 2016.
165 H. Qian, D. Wei and Z. Wang, *Nano Res.*, 2023, **16**, 11718–11730.
166 A. Georgopoulou, D. Hardman, T. G. Thuruthel, F. Iida and F. Clemens, *Adv. Sci.*, 2023, **10**, 2301590.
167 J. H. Lee, J. S. Heo, Y.-J. Kim, J. Eom, H. J. Jung, J.-W. Kim, I. Kim, H.-H. Park, H. S. Mo, Y.-H. Kim and S. K. Park, *Adv. Mater.*, 2020, **32**, 2000969.
168 F. Liu, S. Deswal, A. Christou, Y. Sandamirskaya, M. Kaboli and R. Dahiya, *Sci. Robot.*, 2022, **7**, eabl7344.
169 W. Yin, Y. Xie, J. Long, P. Zhao, J. Chen, J. Luo, X. Wang and S. Dong, *Nano Energy*, 2018, **50**, 16–24.
170 D. Vera Anaya, T. He, C. Lee and M. R. Yuce, *Nano Energy*, 2020, **72**, 104675.
171 S. Chen, N. Wu, L. Ma, S. Lin, F. Yuan, Z. Xu, W. Li, B. Wang and J. Zhou, *ACS Appl. Mater. Interfaces*, 2018, **10**, 3660–3667.
172 D. V. Anaya, K. Zhan, L. Tao, C. Lee, M. R. Yuce and T. Alan, *Nano Energy*, 2021, **90**, 106486.
173 J. Cao, X. Fu, H. Zhu, Z. Qu, Y. Qi, Z. Zhang, Z. Zhang, G. Cheng, C. Zhang and J. Ding, *Small Methods*, 2022, **6**, 2200588.
174 H. Zhou, W. Huang, Z. Xiao, S. Zhang, W. Li, J. Hu, T. Feng, J. Wu, P. Zhu and Y. Mao, *Adv. Funct. Mater.*, 2022, **32**, 2208271.
175 Y. Li, Q. Li, X. Ma, X. Li and Y. Guo, *Nano Energy*, 2025, **133**, 110437.
176 S. A, X. Gao, C. Lu, D. Yao, M. Lu, M. Zhang, Y. Sun, H. Fang and D. Li, *IEEE Sens. J.*, 2022, **22**, 12547–12559.
177 S. Peng, Y. Feng, Y. Liu, M. Feng, Z. Wu, J. Cheng, Z. Zhang, Y. Liu, R. Shen and D. Wang, *Nano Energy*, 2022, **104**, 107899.
178 A. S, X. Gao, C. Lu, D. Yao, M. Lu, M. Zhang, Y. Sun, H. Fang and D. Li, *IEEE Sens. J.*, 2022, **22**, 12547–12559.
179 J. H. Han, K. M. Bae, S. K. Hong, H. Park, J.-H. Kwak, H. S. Wang, D. J. Joe, J. H. Park, Y. H. Jung, S. Hur, C. D. Yoo and K. J. Lee, *Nano Energy*, 2018, **53**, 658–665.
180 G. Ye, Q. Wu, Y. Chen, X. Wang, Z. Xiang, J. Duan, Y. Wan and P. Yang, *Adv. Fiber Mater.*, 2024, **6**, 1874–1886.
181 W. Liu, Y. Duo, X. Chen, B. Chen, T. Bu, L. Li, J. Duan, Z. Zuo, Y. Wang, B. Fang, F. Sun, K. Xu, X. Ding, C. Zhang and L. Wen, *Adv. Funct. Mater.*, 2023, **33**, 2306368.
182 G. Ye, T. Jin, X. Wang, Y. Chen, Q. Wu, Y. Wan and P. Yang, *Nano Energy*, 2023, **113**, 108580.